8-28-2014

Electrospinning of Ceria and Nickel Oxide Nanofibers

Jyothi Swaroop Reddy Yerasi

Electrospinning of Ceria and Nickel Oxide Nanofibers

Jyothi Swaroop Reddy Yerasi

Thesis submitted to the Faculty of the
Rochester Institute of Technology
In partial fulfillment of the requirements for the degree of

Master of Science
In
Industrial Engineering

Thesis Committee

Dr. Denis Cormier

Dr. Marcos Esterman

Department of Industrial and Systems Engineering

08/28/2014

DEPARTMENT OF INDUSTRIAL AND SYSTEMS ENGINEERING

KATE GLEASON COLLEGE OF ENGINEERING
ROCHESTER INSTITUTE OF TECHNOLOGY

ROCHESTER, NEW YORK

CERTIFICATE OF APPROVAL

August 28, 2014

M.S. DEGREE THESIS

The M.S. degree thesis of Jyothi Swaroop Reddy Yerasi

has been examined and approved by the

thesis committee as satisfactory for the

thesis requirement for the

Master of Science degree

Approved by:

Dr. Denis Cormier, Thesis Advisor

Dr. Marcos Esterman, Committee Member

Abstract

Electrospinning uses an electrical charge to draw very fine fibers from a liquid. It has very high potential for industrial processing. Electrospinning is cost effective, repeatable and it can produce long, continuous nanofibers. Polymers such as polyalcohol, polyamides, and PLLA can be easily electrospun. The increase in demand for clean energy combined with the research work in progress and the potential advantages of electrospun electrodes over conventionally fabricated SOFCs makes electrospinning a strong candidate. In this thesis, ceramic nanofibers (ceria and nickel oxide) that can potentially be used in SOFCs are fabricated.

A three-phase approach is implemented in the fabrication of ceria and nickel oxide nanofibers. The first phase involves the preparation of the composite ceramic-polymer solution to be electrospun. The second phase gives the processing conditions such as voltage applied, feed rate, and gauge of syringe tip used for successfully electrospinning composite ceramic-polymer fibers. The final stage demonstrates the temperature cycles used to burn out the polymer and calcine the ceramic particles in the ceramic-polymer nanofibers leaving behind ceria and nickel oxide nanofibers.

Techniques such as scanning electron microscopy (SEM), energy dispersive spectroscopy (EDS) and X-ray Diffraction (XRD) were used to measure the average diameter of the fibers formed and to understand the chemical composition and crystallanity of the nanofibers after calcination. This thesis also discusses the advantages and possibility of fabricating side-by-side nanofibers and oriented nanofiber mats.

Dedication

I dedicate my dissertation work to my family and many friends. A special feeling of gratitude for my loving parents, Rami Reddy and Geethanjali whose words of encouragement and push for tenacity ring in my ears.

I am dedicating this work to my late elder brother Yerasi Aditya Kumar Reddy, gone forever from our loving eyes and left a void that can never be filled. Though your life was short, I will make sure your memory lives on as long as I shall live. I love you and miss you beyond words. May you find peace and happiness in paradise.

Acknowledgement

I would like to express my deep gratitude to Professor Denis Cormier and Professor Marcos Esterman, my research supervisors, for their patient guidance, enthusiastic encouragement and useful critiques of this research work. Without Professor Cormier's input and inspiration, this thesis would not have been possible. I am grateful to have had the opportunity to work on the HeteroFoaM research project. I would also like to thank Professor Richard Hailstone, for his advice and assistance in validating the theory presented in this research work and for capturing SEM images. I would also like to thank Ms. Lyn Irving from Cerion enterprises for her feedback and support in the formulation of GDC ink used in the preliminary experiments. I would also like to extend my thanks towards the Industrial and Systems Engineering Department for their help in offering me the resources in running the program and their support over the last three years. I would also like to thank RIT for its generous support that made this thesis possible.

I would like to thank my fellow Industrial engineering graduate students, roommates and to all who helped me throughout my journey at RIT.

Finally, I would like to thank my father Rami Reddy and mother Geethanjali and my brother Aditya Kumar Reddy for their unwavering faith and support. I would like to give special thanks to my friends for being there for me throughout the entire program.

Table of Contents

Chapter 1 ..... **1**

Introduction **1**

1.1 Solid Oxide Fuel Cell (SOFC) **1**

1.2 SOFC Fabrication **3**

1.3 Nanomaterials and Nanofibers **4**

1.3.1 Applications of Nanomaterials and Nanofibers 5

1.3.2 Fabrication of Nanofibers 6

1.4 Problem Statement **11**

1.4.1 User Controlled Process Parameters 13

1.5 Thesis Objectives **14**

Chapter 2 ..... **16**

Literature Review **16**

2.1 Origins of Electrospinning **16**

2.2 Recent Electrospinning Research **17**

2.3 Electrospinnable Materials **19**

2.3.1 Polymers 19

2.3.2 Composites 20

2.3.3 Ceramics 22

2.4 Electrospinning Process Parameters **22**

2.4.1 Solution Properties 23

2.4.2 Processing Conditions 26

2.4.3 Environmental Parameters 31

Chapter 3 ..... **33**

Methods and Materials **33**

3.1 Experimental Setup **33**

3.2 Experimental Methodology **35**

3.2.1 Ink Preparation 36

3.2.2 Electrospinning and Peeling 36

3.2.3 Post Processing Conditions 38

3.2.4 Analysis 38

Chapter 4 ..... **40**

Experimental Results and Discussion **40**

4.1 Feasibility Tests **40**

4.2 Ceramic-Polymer Solution Preparation **42**

4.3 Electrospinning Ceramic-Polymer Solutions **43**

4.4 Post Processing Conditions **45**

4.5 Results **46**

4.5.1 SEM Images and EDS Data 46
4.5.2 XRD Analysis 50

Chapter 5 54

Conclusions and Recommendations 54
5.1 Summary 54
5.2 Contributions 55
5.3 Future Recommendations 55

Bibliography 59

Appendix A: Sintered ceria XRD data summary 64

Appendix B: Sintered Nickel XRD data summary 65

Appendix C: PDF Card 66
C.1. Cerium oxide PDF Card 66
C.2. Nickel oxide PDF Card 67

List of Figures

Figure 1: Schematic diagram of a SOFC 3
Figure 2: Fabrication of nanofiber by drawing (adapted from (Seeram , et al. 2005)) 7
Figure 3: Fabrication of nanofiber by template synthesis (adapted from (Seeram , et al. 2005)) 8
Figure 4: Generic schematics of phase separation (adapted from (Seeram , et al. 2005)) 9
Figure 5: Schematic diagram of electrospinning process (adapted from (Seeram , et al. 2005)) .. 11
Figure 6: Number of papers with the keyword 'electrospinning' 17
Figure 7: Electrospinning setup in Earl W. Brinkman lab 37
Figure 8: SEM image of as spun PVA nanofibers 40
Figure 9: SEM image of as-spun ceria-Mowiol nanofibers 44
Figure 10: SEM image of as-spun nickel-Mowiol nanofibers 45
Figure 11: Firing schedule for ceramic-Mowiol composite nanofibers 46
Figure 12: SEM images of cerium oxide nanofibers 47
Figure 13: SEM images of nickel oxide nanofibers 47
Figure 14: EDS spectra for as spun cerium-Mowiol nanofibers 48
Figure 15: EDS spectra of sintered ceria nanofibers 49
Figure 16: EDS spectra comparison of as spun and sintered ceria nanofibers 49
Figure 17: EDS spectra for sintered nickel nanofibers 50
Figure 18: XRD data of as-spun and sintered ceria nanofibers 51
Figure 19: XRD analysis of as-spun and sintered nickel oxide nanofibers 53
Figure 20: Method to fabricate parallel or side-by-side fibers by electrospinning 56
Figure 21: Novel method to fabricate parallel or side-by-side nanofibers 57
Figure 22: Chamber design 57
Figure 23: (a) Single Taylor cone achieved by joining two syringe tips using an alligator clip; (b) close-up view 58

List of Tables

Table 1: Electrospinning jet observations and possible causes 14
Table 2: Cerium oxide nanofibers XRD summary 52
Table 3: Nickel oxide nanofibers XRD summary 53

Chapter 1

Introduction

1.1 Solid Oxide Fuel Cell (SOFC)

A fuel cell is a device that typically converts the chemical energy from a fuel into electricity through a chemical reaction with oxygen or another oxidizing agent instead of combustion. Hydrogen is the most common fuel that is used but hydrocarbons such as natural gas and alcohols like methanol are sometimes used as fuels for a fuel cell. Fuel cells are primarily used as backup power for commercial, industrial and residential buildings. They are also used to power fuel-cell vehicles, including forklifts, automobiles, boats and submarines.

Solid oxide fuel cells (SOFCs) use hard ceramic compounds of metal oxides as electrolyte materials. Nickel oxide - cerium samarium oxide, nickel oxide - yttria stabilized zirconia (YSZ), nickel (II) oxide and vanadium (III) oxide can be used as anode materials and gadolinium doped ceria (GDC), samarium doped ceria (SDC), lanthanum germinate and yttria stabilized zirconia (YSZ) can be used as electrolytes. Outputs of SOFC's are as high as 100kW. Efficiencies of SOFC's can reach 60% with operating temperatures approaching 1000^{o}C for some SOFC's. Since SOFC's are used at such high temperatures; reformers that extract hydrogen from the fuel are not always needed. Waste heat can be recycled to make additional electricity. However, the high temperature limits applications of SOFC units, and SOFCs tend to be rather large in size.

SOFCs have several advantages such as their flexibility in the choice of fuels, their efficiency (fuel input to electricity output), low emissions, potential long life expectancy when compared to some other types of fuel cells, and lack of moving parts. SOFC's produce high quality heat as a byproduct that can be used for co-generation.

An SOFC consists of two electrodes sandwiched around a hard ceramic electrolyte such as zirconia or ceria. A general schematic of a solid oxide fuel cell is illustrated in Figure 1. Hydrogen fuel is fed into the anode of the fuel cell. Oxygen from the air enters the cell through the cathode. The anode, cathode and electrolyte in a SOFC serve several functions and therefore have several requirements. They must have proper chemical, morphological and dimensional stability. They should also have high conductivity and must be chemically compatible with other components. The anode and cathode must be porous to allow gas transport to the reaction sites. Since SOFC's are operated at high temperatures, they must have high thermal stability and high strength.

The most commonly used electrolyte materials are samarium doped ceria (SDC), gadolinium doped ceria (GDC), yttria doped ceria (YDC), calcium doped ceria (CDC), lanthanum strontium gallium magnesium (LSGM), bismuth yttrium oxide (BYO), barium cerate (BCN), yttria stabilized zirconia (YSZ) and strontium cerate (SYC). NiO/YSZ anode material is suited for applications with YSZ electrolyte material whereas NiO/SDC and NiO/GDC anode materials are commonly used with ceria-based electrolyte materials. The anode structure is typically fabricated with a porosity of 20-40% to facilitate mass transport of reactant and product gases. Perovskites such as lanthanum strontium manganite (LSM), lanthanum calcium manganite (LCM), lanthanum strontium ferrite (LSF), and samarium strontium cobaltite (SSC) may be used as cathode materials. Similar to the anode, the cathode is a porous structure that must permit rapid mass transport of reactant and product gases. Porous graded anode substrates for solid oxide fuel cells are considered to optimize the gas transport through the substrate by maintaining high electrochemical activity for fuel oxidation at the anode/solid electrolyte interface (Holtappels, et al. 2006).

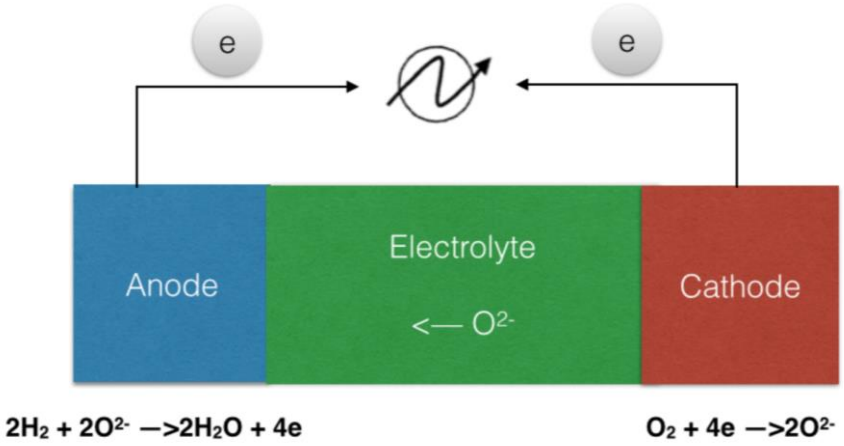

Figure 1: Schematic diagram of a SOFC

1.2 SOFC Fabrication

Screen printing and tape casting are two of the most favored techniques for fabricating SOFC layers. The conventional method for producing Ni/YSZ cermets involves high-temperature sintering of printed NiO and YSZ pastes, followed by reduction of the resulting composite to form Ni from the NiO (Virkar, et al. 2000). Sintering temperatures are typically on the order of 1350°C to have the YSZ within the composite form to form a continuous phase.

SOFC anode and cathode layers are typically required to be porous. The porous layer can be produced by tape casting pastes that include organic pore formers that burn off during sintering. An alternate approach is to chemically leach out pore formers after printing. In the literature, NiO and Ceria were added to the porous YSZ matrix via wet impregnation of nitrate salts (Gorte, et al. 2000).

Tortuosity is a property of porous materials that is used to indicated whether gas/liquid flowing through the porous material has a relatively straight path (i.e. low tortuosity) or a highly twisting and convoluted path (i.e. high tortuosity). Usually subjective estimation is used to measure tortuosity in 3-D. However, several methods can be used to quantify tortuosity such as arc-chord ratio, arc-chord ratio divided by the number of inflection points and integral of square curvature,

divided by length of the curve (Bullitt, et al. 2003). Another method used for quantifying tortuosity in 3D has been applied in 3D reconstructions of solid oxide fuel cells cathodes where the Euclidean distance sums of the centroids of a pore were divided by the length of the pore (Gostovic, et al. 2007). Tortuosity of an anode can be defined as a ratio of the real diffusion path length and electrode thickness. Carman (Carman 1937), who studied flow through a bed of sand, first introduced the concept of tortuosity to a porous media. He introduced tortuosity as a factor that takes into account the elongated diffusion path of fluid inside porous media. Porosity is a measure of the void spaces in a material, and is a fraction of the volume of voids over the total volume, or as a percentage between 0 and 100%. Methods such as CT scanning can be used to test the porosity in a substance or part.

Electrospun fibers collected on a flat collector potentially have high tortuosity. But nanofibers with high porosity can also be fabricated by aligning fibers using a modified collector setup. When fibers are aligned perpendicular to each other using a grid collector such as a conductive screen material, the porosity of the electrospun mat increases. Electrospun nanofibers have potential high surface areas and high triple phase boundaries when compared to conventionally fabricated SOFCs, hence the review now turns to a study of nano-fibrous materials.

1.3 Nanomaterials and Nanofibers

Nanomaterials have been the subject of intensive research for many years. One-dimensional nanostructures have been of special interest due to their unique properties and applications in many areas. Among the first application of nanomaterials was glazes for porcelain in the early Chinese dynasty. There are instances of artists from the renaissance period using nanomaterial in art. The idea of nanotechnology was first introduced in 1959 when Richard Feynman, a physicist at Caltech, gave a talk called "There's Plenty of Room at the Bottom" (Feyman 1959). He presented the idea that eventually it would be possible to precisely manipulate atoms and

molecules. In 1979, Dr. K. Eric Drexler who was inspired by Feynman's talks put these concepts into motion by expanding Feynman's vision. He promoted the technological significance of nanoscale phenomena and devices through his speeches and his books “Engines of Creation: The Coming Era of Nanotechnology (1986)” and “Nano systems: Molecular Machinery, Manufacturing and Computation” (1992), and so the term acquired its current sense.

Nanofibers can be considered as two separate words “nano” and “fibers”. Historically “nano” is used to describe anything within a scale of 10^9 of the reference unit (e.g. nanometer, nanogram etc.). The word fiber has different meanings from various professional viewpoints. In this particular study, a fiber is defined from a geometrical standpoint and is defined as a slender, elongated, threadlike object or structure.

1.3.1 Applications of Nanomaterials and Nanofibers

Several amazing characteristics, such as superior mechanical properties and very large surface area to volume ratio, are brought into light when the diameters of the fiber materials are in the nanoscale regime. These outstanding properties make polymer nanofibers suitable candidates for many important applications. Some of the applications of these polymer nanofibers are in the areas of defense and security, energy devices, electronics, bioengineering, environmental engineering and biotechnology.

Nanofibers have applications in medicine, including artificial organ components, tissue engineering, drug delivery and implant materials. Protective nano-fiber materials include sound absorption materials, protective clothing against chemical and biological warfare agents, and sensor materials for the detection of chemical agents. They are also used in the manufacturing of sports apparel, rainwear, baby diapers and outerwear garments in the textile industry. Many HVAC (heating, ventilating and air conditioning) system filters, HEPA (high efficiency particulate air) filters, air, oil, fuel filters for automotive and filters for vacuum cleaners are made

using nanofibers. Energy applications include Li-ion batteries, photovoltaic cells, membrane fuel cells, and dye-sensitized solar cells. Other applications include micro power to operate personal electronic devices via piezoelectric nanofibers woven into clothing, carrier materials for various catalysts, and photo catalytic air/water purification. Ceramic nanofiber mats can also be used as electrodes of a solid oxide fuel cell (Mingjia, et al. 2012). A 3D nanofiber electrode has several advantages such as high surface area, high percolation, a continuous pathway for charge transportation, and good thermal stability at high operating temperatures.

1.3.2 Fabrication of Nanofibers

Numerous techniques such as drawing, template synthesis, phase separation, and electrospinning can be used to prepare nanofibers (Seeram , et al. 2005).

1.3.2.1 Drawing

Ondarcuhu and Joachim (1998) describe a process where a micropipette with a diameter of a few micrometers was first dipped into a droplet near the contact line using a micromanipulator. The micropipette was then withdrawn from the liquid and moved at a speed of approximately $1*10^{-4}$ ms^{-1}, resulting in a nanofiber being pulled (Ondarcuhu and Joachim 1998). The fibers were deposited on the surface by touching them with the end of the micropipette. Several nanofibers can be prepared from a single droplet. Nanofibers can be drawn with dimensions comparable with the ones of single-wall carbon nanotubes. The process is illustrated in Figure 2.

Some advantages of this process include low equipment costs, process repeatability and convenience. Some potential limitations of the process are that it produces discontinuous fibers, the dimensions of the fibers may be difficult to control, and the process may be difficult to scale up to commercial volumes.

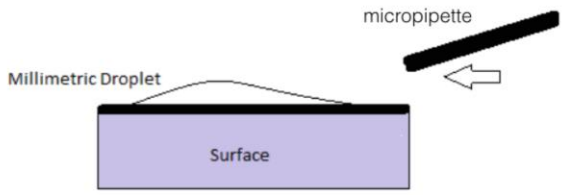

Step 1: Micropipette is moved towards the contact line of the droplet

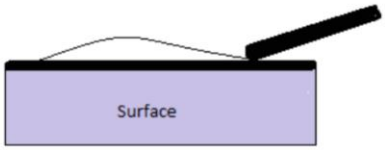

Step 2: Micropipette comes in contact with contact line

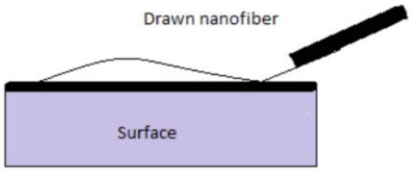

Step 3: Micropipette is withdrawn producing nano fiber

Figure 2: Fabrication of nanofiber by drawing (adapted from (Seeram , et al. 2005))

1.3.2.2 Template Synthesis

Template synthesis of nanomaterials has fascinated many scientists due to its simplicity and diverse applications. Different methods such as electrochemical deposition, sol-gel and chemical vapor deposition can be combined with the template synthesis technique to fabricate different types of materials (e.g. metals, carbons, semiconductors, metal oxides, conductive polymers etc.). Template synthesis is widely used in fabricating heterogeneous nanostructures such as composite nanowires, segmented nanowires, and coaxial nanowires. The word template synthesis implies that the process makes use of a template or mold to obtain a desired material or structure.

The membrane with nanopores in Figure 3 acts as a mold, whereas the polymer solution acts as the raw material to the process. When water is in contact with the polymer, the pressurized polymer solution extrudes through the nanopores in the membrane. These nanofibers solidify to form nanofibers (Feng 2002). There are a few things that need to be taken into consideration

while building a template. The lifetime of the template must be greater than the reaction time, and the template must offer chemical or energetic contrast for incoming reagents.

Some advantages of this process include its repeatability, relative simplicity, and ability to have reasonable control over fiber diameters. Designing large porous membranes capable of withstanding high pressures may be difficult, thus making it challenging to scale-up to production quantities.

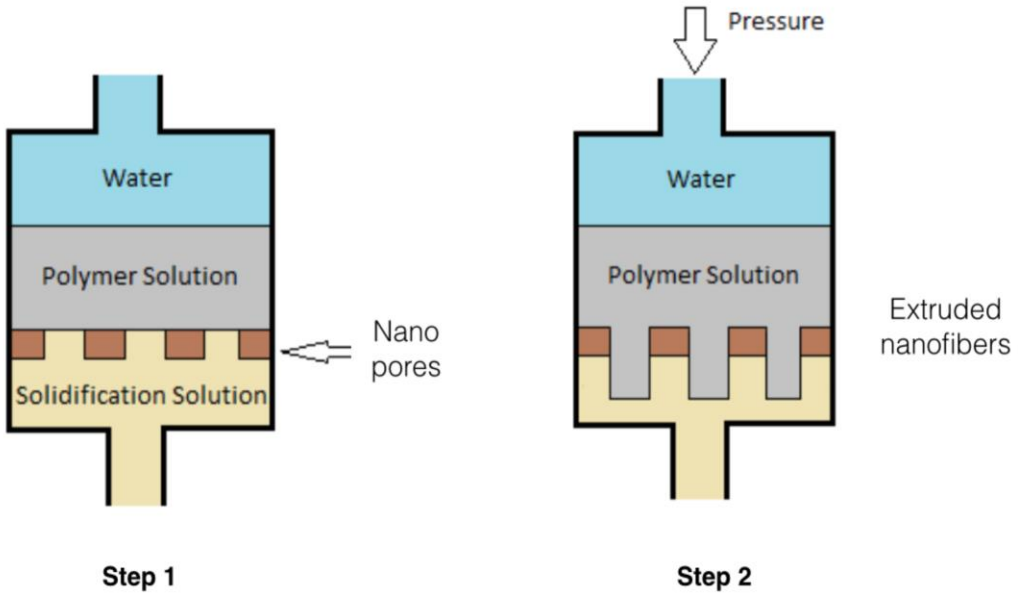

Figure 3: Fabrication of nanofiber by template synthesis (adapted from (Seeram , et al. 2005))

1.3.2.3 Phase separation

In phase separation, a polymer is first mixed with a solvent before undergoing gelation. The main mechanism in this process is the separation of phases due to physical incompatibility. One of the two phases, that of the solvent, is then extracted leaving behind the other phase. The major steps in this process are (1) polymer dissolution, (2) gelation and (3) solvent extraction (Ma 1999) as shown in Figure 4.

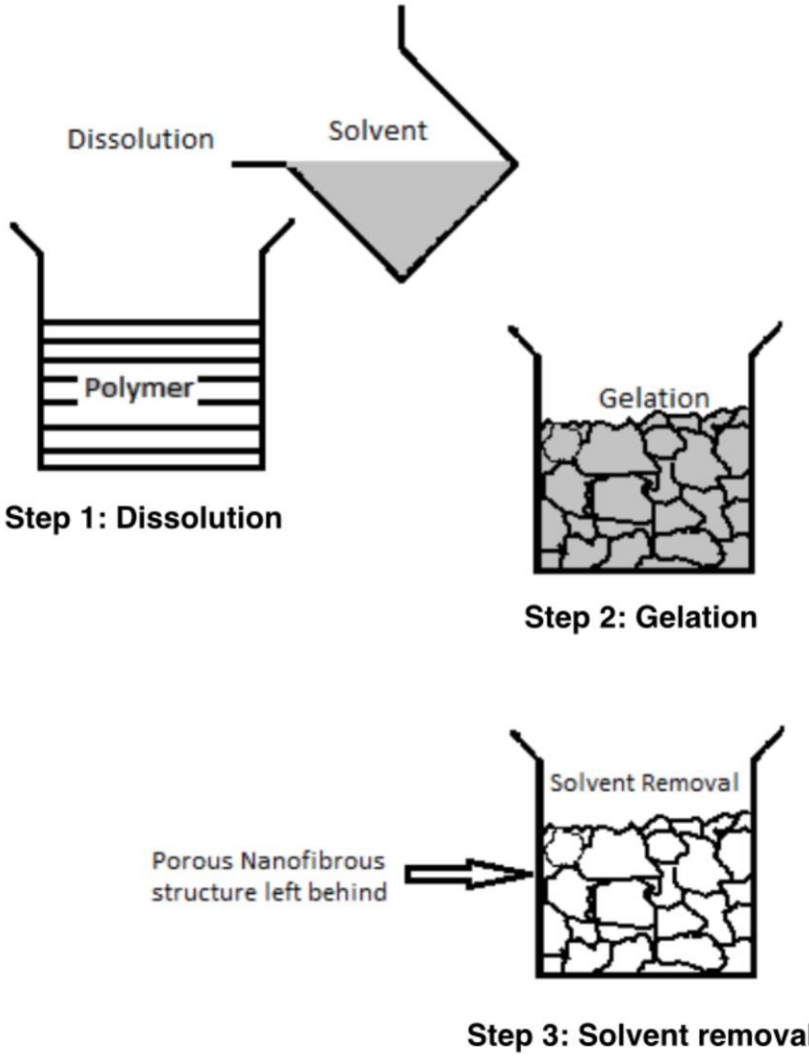

Figure 4: Generic schematics of phase separation (adapted from (Seeram , et al. 2005))

Some advantages of this process include repeatability, ease of processing, its ability to produce continuous nanofiber networks, control over polymer concentrations, and batch-to-batch consistency. Some challenges with the process are that it may be difficult to control fiber dimensions, and the process may be difficult to adapt for use with ceramic materials.

1.3.2.4 Electrospinning

Electrospinning is a process that creates nanofibers through an electrically charged jet of polymer solution or polymer melt. This process in its simplest form consists of a pipette to hold the polymer solution, two electrodes and a DC voltage supply of the order of kilovolts. The first electrospinning patent appeared in 1934 when Formhals disclosed an apparatus for producing polymer filaments that took advantage of the electrostatic repulsions between surface charges (Formhals, Process and apparatus for preparing artificial threads 1934).

Unlike the other methods for generating 1D nanostructures, fiber formation in electrospinning is based on uniaxial stretching. The polymer droplet formed at the tip of the pipette is drawn into nanofibers due to a very high voltage applied across it. The jet is electrically charged, and the charge causes the fibers to stretch in such a way that their diameters reduces. The fibers are collected on a grounded surface referred to as the target.

When compared with mechanical drawing, electrospinning is more suitable for generation of fibers with thin diameters. This is possible since the elongation in this process is a result of a contactless scheme through the application of an external electric field.

Electrospinning is a continuous process and can be considered as a variant of the electrostatic spraying process. In electro spraying, small droplets of the polymer are formed as a result of the break-up of the jet and are collected on the grounded target. In electrospinning, continuous nano fibers are collected at the target.

For a polymer to be electrospun into fibers, a suitable solvent should be available for dissolving the polymer. The vapor pressure of the solvent should be suitable so that it evaporates quickly to maintain the integrity of the fibers as they approach the target but not so quickly that it allows the fibers to harden before they reaches the target. The viscosity and surface tension of the polymer solution should not be too large or too small. Excessively large viscosity prevents the jet from

forming, whereas excessively low viscosity allows the polymer solution to drain freely from the pipette. The power supply should be adequate to overcome the viscosity and surface tension of the polymer solution to form and sustain the jet from the pipette. The gap between the tip of the pipette and the substrate must be large enough to prevent electrical discharge. Likewise, the gap should not be so large that the solvent evaporates before the fibers form.

Advantages of electrospinning include the ability to produce long continuous nanofibers, low cost, scalability, repeatability, and ease of control. The process is illustrated in Figure 5. The ability to produce continuous nanofibers makes electrospinning an ideal candidate for the fabrication of ceramic nanofibers that can be used in applications such as SOFC's.

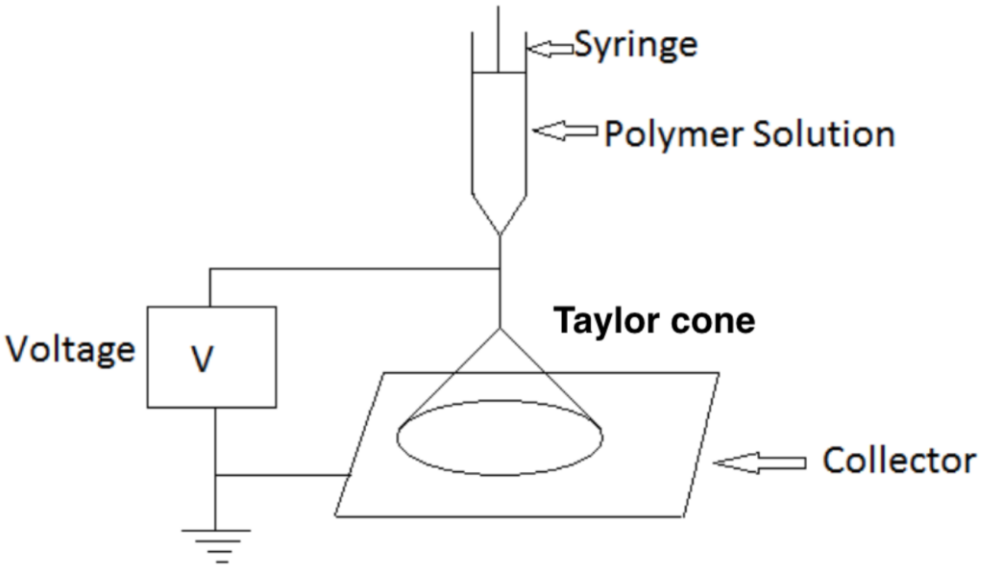

Figure 5: Schematic diagram of electrospinning process (adapted from (Seeram , et al. 2005))

1.4 Problem Statement

Networks of continuous nanofibers are of considerable interest in nanoscience and nanotechnology due to exceptional properties that make them suitable for many potential applications as previously mentioned. Some ceramics have wide applications with field effect

transistors, catalysis, photo electrolysis reactors, batteries, magnetic storages and gas sensors. Nanofibers can also be used where a large surface area is required. Some ceramic nanofibers are used in industrial applications as well. There have been instances in the literature where ceramic nanofibers were fabricated by electrospinning processes.

Nanofiber networks of two materials, cerium oxide and nickel oxide, are of particular interest for this research. Cerium oxide (i.e. ceria) nanofibers loaded with noble materials are promising catalysts for the elimination of noxious auto-exhaust gases (Bleiwas 2013). Flower-like ceria microspheres can also be used for the production of hydrogen from biomass-derived alcohol (Chunwen, et al. 2006). These fibers can also be used in the fabrication of solid oxide fuel cells due to their potential for providing clean and reliable electric power. It has been reported that ceria-based ion conductors have a high resistance to carbon deposition, which permits the direct supply of dry hydrocarbon fuels to the anode (Seungdoo, John and Raymond 2000). They also have applications in sensors, photocatalysis and biomedical fields. Nickel oxide nanofibers can be used for preparing the anode layer of solid oxide fuel cells. They can also be used in fabricating nickel oxide cathodes of lithium ion micro batteries, light weight aerospace structural components, active optical fibers, cathode materials for alkaline batteries, P-type transparent conductive films and gas sensors.

This thesis discusses and showcases electrospinning in the fabrication of composite nickel-polymer and ceria-polymer nanofibers. It also gives the post processing steps involved in the synthesis of continuous cerium oxide (ceria) nanonetworks and nickel oxide nanonetworks.

The objectives of this thesis can be divided into three major categories. The first objective was to build an electrospinning setup, display the ability of this setup to electrospin nanonetworks, and understand the science behind electrospinning and the various factors involved. The second objective was to determine the suitable composition of nickel and ceria electrospinning solutions.

The third objective was to separate the nanofibers from the aluminum foil and determine the temperature cycles at which polymer material could be burned out without compromising the morphology and the structure of the ceramic nanofibers. Finally, characterization of nanofiber networks via the scanning electron microscope (SEM), electron discharge spectroscopy (EDS) and X-ray diffraction (XRD) methods was needed.

Process parameter values used with the electrospinning setup dictate the diameter and morphology of the fibers fabricated. Depending on the application, one might need to control the diameter and morphology of the fibers. For example, if an application requires hollow nanofibers, then a coaxial syringe tip may be used, and the other process parameters must be optimized so that desired results are achieved. A large part of research conducted on electrospinning deals with its application to fields such as bioengineering, filters and solid oxide fuel cells. However, research that involves the fabrication of cerium and nickel oxide nanofibers has not yet been extensively presented in literature. The primary goal of this thesis is to give a process for the fabrication of cerium and nickel nanofibers.

1.4.1 User Controlled Process Parameters

The output of the electrospinning setup is controlled by varying several parameters such as syringe tip diameter, distance between the syringe tip and the collector, viscosity of the solution, solid loading fraction of the solution, and feed rate. Controllable parameters of the electrospinning system are as follows.

1. **Feed Rate** (ml/hr) - flow rate of the solution exiting the syringe tip.

2. **Syringe Tip Size** (Gauge) - influences the diameter of the fiber. When the distance between the collector and syringe tip is the same, larger diameter syringe tips form fibers with larger diameters.

3. **Ink Viscosity** (cP) – affects the flow of the ink throughout the electrospinning cycle.

4. **Offset Distance** (mm) – the distance between syringe tip and collector influences the diameter of the fibers and morphology of electrospun fibers.

5. **Solid Loading Fraction** (wt %) - affects the viscosity of the solution and greatly affects the ability of the spun fibers to be thermally decomposed into pure ceramic fibers.

Some effects of individual parameters or a combination of parameters on the electrospinning jet are discussed in Table 1.

Table 1: Electrospinning jet observations and possible causes

Observation	Description	Possible Causes
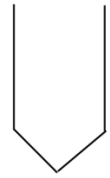	No solution out of the syringe tip; No Electrospinning	Solution too viscous. Bubbles in the solution.
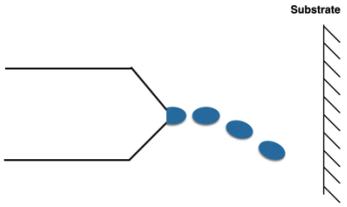	Solution not reaching the substrate; Electrospraying instead of electrospinning; Dripping; Spitting small globs	Solution not viscous enough; Voltage is too low; Distance between the collector and syringe tip is too large; Low polymer percentage.
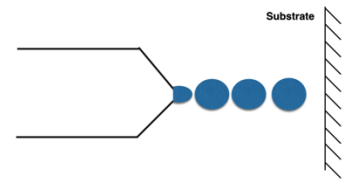	Spitting large globs or beads Clumping at the tip	Solution viscosity is too high; Voltage too high;

1.5 Thesis Objectives

As discussed previously, this thesis aims to showcase the ability to fabricate continuous, rather than discrete, ceria and nickel oxide nanonetworks by electrospinning. Both ceria and nickel oxide plays a major role as functional materials in the preparation of solid oxide fuel cells. Electrospun electrodes have potential advantages such as high porosity, provision of continuous pathways for charge transportation, high percolation, high surface area, and higher triple phase

boundary length. The objective of this thesis is to develop a procedure for the fabrication of continuous ceramic (ceria and nickel oxide) nanofiber networks that can be used in applications such as solid oxide fuel cells. Procedures to prepare electrospinning solutions, parameters required for electrospinning these solutions, procedure to peel the composite nanofiber mat off of the collector, and the post processing conditions required to synthesize ceria and nickel oxide nanofiber networks have been developed. Scanning electron microscopy (SEM) images, electron discharge spectroscopy (EDS) data and X-ray diffraction (XRD) data have been captured to characterize the synthesized ceramic nanofibers. This thesis also sheds light on the process to fabricate parallel, or side-by-side, fibers using a modified setup.

Chapter 2

Literature Review

2.1 Origins of Electrospinning

In the late 1500's, William Gilbert set out to describe the behavior of magnetic and electrostatic phenomena. Little was he aware that his discovery would become a modern scientific method. He distinguished between the magnetic forces arising from a loadstone (natural magnet) and the electrostatic force arising from rubbed amber. One of his more obscure observations was that when a suitably charged piece of amber was brought near a droplet of water it would form a cone shape and small droplets would be ejected from the tip of the cone. This is perhaps the first recorded observation of electrospraying.

The first description of a process recognizable as electrospinning was in 1902 when J.F. Cooley filed a US patent 'Apparatus for electrically dispersing fibers' (Cooley 1902). In his patent (US 692631), he described a method of using high voltage power to generate yarn. Even at such an early stage, it was recognized that in order to form fibers instead of droplets, the fluid must be sufficiently viscous, the solvent should be volatile enough to evaporate to allow regeneration of solid polymer, and the electric field should be within a certain range. In 1914, John Zeleny (Zeleny 1914) published his work on the behavior of fluid droplets at the end of metal capillaries. His work began the trend to mathematically model the behavior of fluids under electrostatic forces. Between 1964 and 1969, Sir Geoffrey Ingram Taylor worked on the underlying phenomenon of electrospinning (G.Taylor 1964). Taylor's work of mathematically modeling the shape of cone formed by the fluid droplet under the effect of an electric field has contributed greatly to electrospinning. This characteristic droplet shape is now known as the "Taylor cone". Norton proposed melt spinning and air-blast assist processing which were low throughput and simpler. Anton Formhals filed a patent (Formhals, Artificial thread and method of producing

same 1940) on constant pressure feed high-throughput machines to produce continuous fine fibers for use on standard textile machinery.

2.2 Recent Electrospinning Research

Using the keyword ‘electrospinning’ for searches in scientific databases (Compendex and Inspec) returned about 21,500 papers (search performed on 10/15/2014, range 1884-2014. Figure 6 shows a plot of the number of scientific journal and article papers published per year since 2000. This graph demonstrates the recent strong growth in this area. Use of the same keyword for a search in the U.S. patent database returns about 14,680 documents at the time of this writing. Given that there are only a handful of companies that produce electrospinning equipment or products, there is a need for focused electrospinning research on specific applications.

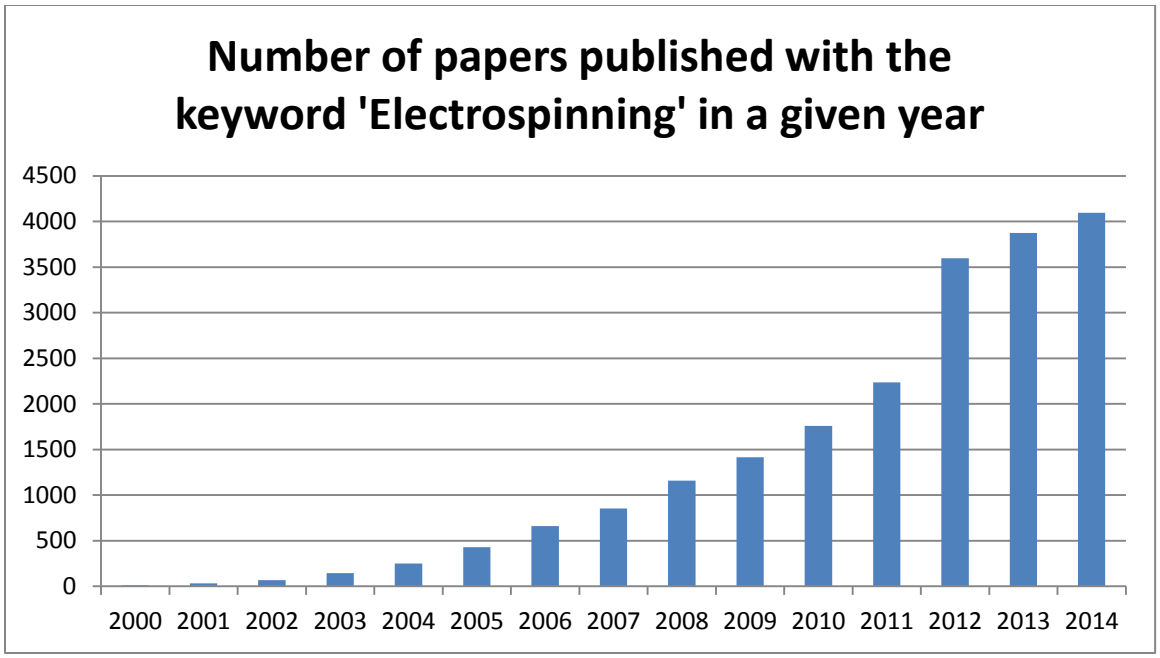

Figure 6: Number of papers with the keyword 'electrospinning'

Electrospinning was re-discovered around 1995 when Chun and Reneker (Reneker and Chun 1996) accidentally observed that this process could easily form fibers of nanometer size range. In a study by Won et al., (2004), solutions were prepared by dissolving polyethylene glycol (PEG)

in chloroform, ethanol, dimethyl form amide and water respectively. When these solutions were electrospun, it was observed that the solutions formed with chloroform and ethanol fibers were formed in lower concentration than when dissolved in water. In this study, it was also observed that the addition of polyelectrolytes (salts) would reduce the diameter of fibers. In a paper published in the American Ceramic Society journal (Von Hagen, et al. 2011) vanadium oxide fibers were electrospun and dried in vacuum overnight. One set of fibers was calcined at 600 °C in air for 5 hours. The other set was calcined at 500 °C in N_2 for 5 hours and then post calcined in air for 5 hours at 600 °C in air. It was observed that there was a better control over the morphology of fibers when there were two distinct calcination processes.

A study by Thompson et al. (2007) showed that initial jet radius, volumetric charge densities, distance from nozzle to collector and relaxation time had very strong effects on the diameter and morphology of the fibers. Whereas, initial polymer concentration, solvent vapor pressure, solution density, and electric potential had a moderate effect on the diameter of the fibers, the relative humidity had a very small effect on the diameter of the fibers (Thompson, et al. 2007).

In the literature, two different kinds of setups are commonly described based on the geometrical arrangement of ejecting capillary and collection target: the horizontal type and the vertical type. Further, two kinds of vertical setups are possible: the shaft type and the converse type. In a horizontal type electrospinning setup, the ejecting capillary is horizontal with respect to the ground, and the electrospinning collector plate is in a vertical orientation (i.e. perpendicular to the ground). In a vertical electrospinning setup, the ejecting capillary is vertically oriented parallel to the gravitational force, and the collector plate is horizontally oriented parallel to the ground. If the gravitational force is in the direction of the ejecting capillary (i.e. downward electrospinning), then the setup is considered to be of the shaft type. If the gravitational force acts in the opposite direction, then the setup is said to be of the converse type. Cuiru et al. (2009) observed that the thinnest fibers were formed when they were electrospun by a vertical type

system. It was believed that gravity enhanced the effect of the electric field to make the fibers extend sufficiently. The shaft type system yielded fiber of minimum diameter, but they exhibited very large size variations. The converse type electrospinning system yielded fibers of maximum diameter, but had the minimum size variation of all the three setups (Cuiru, et al. 2009).

In a study by Ying et al. (2007), it was determined that fiber diameter was not decided by solution rate as much as by electric force/unit mass and solvent volatilization. In another study, it was found out that the molecular weight of the solvent had an effect on the morphology of the final fibers. Polyvinyl alcohol (PVA) of three different molecular weights was used for this study. When solutions were prepared and electrospun, fibers made from the lowest molecular weight PVA solution stabilized, whereas the fibers formed with high molecular weight PVA solution had flat fibers. The study also indicated that to electrospin at low voltages, low surface tension solutions were desirable (Koski et al., 2004)

2.3 Electrospinnable Materials

The materials and applications of electrospinning are numerous and of wide scope. Individual material properties must be considered based on the application and availability of the material. Electrospinning processes can be modified to some extent based on the material and the requirement of the fibers. In the production of ceramic fibers, post processes are required after the fibers are electrospun. Thus it is important to have a basic understanding of the different groups of materials before selecting the appropriate electrospun fibers for specific applications.

2.3.1 Polymers

Polymers consist of long chains of molecules with repeating units called monomers that are mostly covalently bonded to one another. Polymers exhibit several properties that are attractive for many applications. Most polymers are inexpensive, as they contain simple elements and they are relatively easy to synthesize. They have found applications in many areas such as clothing,

food packing, medical devices and aircraft. Natural polymers such as silks and collagen have found usage in many tissue engineering applications.

As polymer chains are made of repeating units, the molecular weight of the polymer is the sum of the molecular weight of the individual monomers. Generally, a high molecular weight increases the polymer's resistance to solvent dissolution. The molecular weight of the polymer also has a direct influence on its viscosity.

One of the greatest potential applications of electrospun fibers is the area of bioengineering. For many biomedical applications, the materials used should be biocompatible, thus natural polymers have an advantage over synthetic polymers. Since most natural polymers can be degraded by naturally occurring enzymes, they play a major role in drug delivery and artificial implants. It is also possible to control the rate of degradation by cross-linking or other chemical modifications. Most polymers that have been electrospun are proteins and polysaccharides. Proteins that have been electrospun include collagen (Matthews, et al. 2002), gelatin (Huang, et al. 2004), fibrinogen (Wnek, et al. 2003) and silk (Jin, et al. 2002).

Till date, there are many polymers that have been electrospun including custom made polymers. Many non-biodegradable synthetic polymers made with suitable solvents and concentrations yield smooth fibers without beads. Electrospun fibers are commonly used in the field of tissue engineering due to their small diameters, which are able to mimic natural extracellular matrix. Thus there are two groups of polymers that are commonly electrospun. These are the biodegradable polymers and natural polymers. Many different types of polymers from these two classes have been successfully electrospun, thus highlighting the versatility of electrospinning.

2.3.2 Composites

Composites are combinations of two distinct material phases, a matrix and a reinforcement phase. It is the combination of the strength of the reinforcement and the toughness of the matrix that

gives composites their superior properties that are not available in any single conventional material. Both matrix and reinforcement phases can be metal, ceramic or polymer. Generally, the matrix binds the reinforcement together to give the composite its shape, surface texture and resistance to surroundings. In most cases, composites are designed for load bearing applications, although there are other classes of materials that are used for their interesting electrical, thermal or magnetic properties.

Composites can be classified based on the matrix material and reinforcing material structure. Examples include metal matrix composites (MMC), ceramic matrix composites (CMC), and polymer matrix composites (PMC). MMC's are composed of a metallic matrix (e.g. aluminum, magnesium, iron, cobalt, and copper) and a dispersed ceramic or metallic phase. CMC's are composed of a ceramic matrix and embedded fibers of other ceramic or metal material. PMC's are composed of a matrix of thermoset or thermoplastic material and embedded reinforcements (e.g. glass, carbon, steel or Kevlar fibers).

Based on the reinforcing material structure, there are generally two types of composite reinforcements, fibrous reinforcements and particulate reinforcements. In fibrous reinforcements, the fiber arrangement can take many different forms. The simplest arrangement of fibers in the matrix is to have the fibers aligned in a certain orientation to form a laminate composite. Thin sheets of unidirectional composites can be stacked in an arrangement such that the fibers are oriented. Depending on the application of the composite, different fiber arrangements are used as reinforcement for composite where high torsional stiffness is desired. Randomly distributed fibers in the form of non-woven mat can also be used as reinforcement in composites. In particulate reinforcement, the reinforcing phase has roughly equal dimensions in all directions. The materials are known as aggregate composites. Nanofiber composites of nylon 6 with closite 30B (Fong, et al. 2002) and polyimide with single wall nanotubes (Park, et al. 2001) have been fabricated by electrospinning.

2.3.3 Ceramics

Unlike polymers, electrospun ceramics require an additinoal post-electrospinning process. Ceramic nanofibers can be made by electrospinning of the ceramic precursor and then sintering the electrospun fibers to derive ceramic fibers. Ceramics are materials that commonly exist as compounds of metal oxides, nitrides and carbides. While most ceramics are crystalline, there are amorphous ceramics such as window glass that are made primarily of silicon dioxide. As there are no free electrons in ceramics, they are excellent insulators. The strong ionic and covalent bonding gives ceramics many advantages such as high temperature stability, resistance to chemical attacks, and absorption of foreign matter. Their rigid configuration also gives ceramics their brittleness.

With advances in technology, ceramics are no longer just used for their traditional applications, which largely depend on the insulating properties and mechanical hardness. Ceramics such as calcium carbonate-based ceramics and hydroxyapatite ceramics have found uses as biomaterials (Niklason 2000). A few modifications have been made to the electrospinning process to fabricate ceramic nanofibers. There have been instances where post electrospinning steps such as sintering were added to attain certain results. Sintering conditions significantly influence the reaction of ceramic precursors and the structure of ceramic nanofibers. The most frequently electrospun ceramics are titanium dioxide (TiO_2), silicon dioxide (SiO_2), zirconium dioxide (ZrO_2), aluminum oxide (Al_2O_3), lithium titanate ($Li_4Ti_5O_{12}$), and titanium nitride (TiN).

2.4 Electrospinning Process Parameters

Electrospinning requires process parameters to be within a specified range. Parameters can be broadly classified as pertaining to solution properties, processing conditions and ambient parameters.

2.4.1 Solution Properties

In order to carry out electrospinning, the polymer must first be in a liquid form, either as molten polymer or as a polymer solution. Physical properties of the polymer solutions play a significant role in the electrospinning process and the resultant fiber morphology.

2.4.1.1 Solution Concentration

The concentration of polymer solution used in electrospinning plays a major role in the morphology of the electrospun fibers. Dietzel et al. (2001) state that a solution can be considered to be at one of the four critical concentrations: very low, low, ideal or very high. When the concentration of the solution is very low, discrete polymeric nanoparticles are deposited on the collector, and electrospraying occurs instead of electrospinning (Dietzel, et al. 2001). This is due to the low viscosity and high surface tension of the solution.

If the solution concentration is in the low region, then a mixture of beads and fibers will be collected (Eda and Shivkumar 2007). Smooth nanofibers are obtained when the concentration of the polymer solution is ideal (Eda and Shivkumar 2007). If the concentration is very high, then helix-shaped flat ribbons may be observed (Yang, et al. 2004).

2.4.1.2 Surface Tension

Surface tension is the property of a liquid that allows its surface to resist an external force. The most common quantitative index of surface tension (ξ) is defined by the force exerted in the plane of the surface per unit length. Surface tension is an important factor in electrospinning. It can be treated as a function of solvent composition of a solution. Yang et al. (2004) found that different solvents significantly affect the surface tension of electrospinning solutions. With the solution

concentration fixed, smooth fibers could be obtained rather than beaded fibers if the surface tension of the solution was reduced.

Solvents such as ethanol have a low surface tension and can be added to encourage the formation of smooth fibers. Another way to reduce surface tension is to add surfactant to the solution. The addition of surfactant was found to yield more uniform fibers. Even when insoluble surfactant is dispersed in a solution as fine powders, the fiber morphology can be improved (Zeng, et al. 2003).

2.4.1.3 Molecular Weight and Solution Viscosity

Molecular weight of the polymer also has an important effect on morphologies of electrospun fibers. In theory, molecular weight is related to entanglement of polymer chains in the solution. When keeping the polymer concentration constant, lowering the molecular weight of the polymer tends to form beads rather than smooth fibers. On the other hand increasing the polymer's molecular weight increases the chances of smooth fibers. Further increasing the molecular weight, fibers with flat ribbons will be formed (Koski et al., 2004).

Researchers have also shown that excessively high molecular weight at low concentrations also favors micro-ribbon like morphologies (Zhao, et al. 2005). It is also important to understand that molecular weight is not always essential for electrospinning if sufficient intermolecular interactions can be supplied by oligomers. Oligomers are molecular complexes that consist of several monomer units.

One of the factors that affect the viscosity of the solution is the molecular weight of the polymer. Generally, when a polymer of higher molecular weight is dissolved in a solvent, its viscosity will be higher than solutions of the same polymer having a lower molecular weight. One of the conditions necessary for electrospinning to occur where fibers are formed is that the solution must consists of polymer of sufficient molecular weight, and the solution must be of sufficient

viscosity. During the stretching of the polymer solution, it is the entanglement of the molecule chains that prevents the electrically driven jet from breaking up thus maintaining a continuous solution jet. As a result, monomeric polymer solution does not form fibers when electrospun. The polymer chain entanglements have a significant impact on whether the electrospinning jet breaks up into small droplets or electrospun fibers containing beads. Although a minimum amount of polymer chain entanglement is necessary for electrospinning, a viscosity that is too high will make it very difficult to pump the solution through the syringe needle. Moreover, when the viscosity is too high, the solution may dry at the tip of the needle before electrospinning can be initiated. Experiments have shown that the polymer solution should have minimum viscosity to yield fibers without beads (Megelski, et al. 2002). At low viscosity, it is common to find beads along the fibers deposited on the collection plate. When the viscosity increases, there is a gradual change in the shape of the beads from spherical to spindle like until a smooth fiber is obtained. With increased viscosity, the diameters of the fibers also tend to increase (Jarusuwannapoom, et al. 2005). This is probably due to the greater resistance of the solution to be stretched by the charges on the jet. During electrospinning, there is a possibility of having a secondary jet that is stable enough to yield very fine fibers. This is the reason why two distinct fiber diameter ranges are observed in some cases. However, when the viscosity is high enough, it may discourage secondary jets from breaking off from the main jet, thus contributing to the increased fiber diameter.

2.4.1.4 Solution Conductivity

The polymer type, solvent used, and salts added to the solution determine the electronic conductivity of the solution. Electrospinning involves stretching of the solution caused by the repulsion of the charges at its surface. Thus if the conductivity of the solution is increased, more charges can be carried by the electrospinning jet. The conductivity of the solution can be increased by the addition of ions. If the solution is not stretched properly, then beads might form.

When a small amount of salt or polyelectrolyte is added to the solution, its conductivity increases. As a result, smooth fibers are formed which could otherwise yield beaded fibers. The presence of ions increases the conductivity of the solution while reducing the critical voltage for electrospinning to occur (Son, et al. 2004). Another effect of the increased conductivity is that it results in a greater bending instability. As a result, the deposition area of the fibers is increased (Choi, et al. 2004). Solutions prepared using solvents of higher conductivity generally yield fibers without beads. No fibers are formed if the solution has zero conductivity (Jarusuwannapoom, et al. 2005). The size of the ions may influence the fiber morphology. Ionic surfactants such as tri ethyl benzyl ammonium chloride can be added to increase the conductivity of the solution while simultaneously reducing the surface tension (Zeng, et al. 2003).

2.4.2 Processing Conditions

Other important parameters that affect the electrospinning process include the voltage supplied, the feed rate, temperature of the solution, type of collector. These are explained as follows.

2.4.2.1 Voltage

A crucial element in electrospinning is the application of a high voltage to the solution. The high voltage induces the necessary external electric field to initiate the electrospinning process when the electrostatic force in the solution overcomes the surface tension of the solution. Generally, a voltage potential of more than 6kV is sufficient to initiate a Taylor cone during electrospinning. Depending on the feed rate of the solution, a higher voltage may be required so that the Taylor cone is stable. The columbic repulsive force in the jet will then stretch the viscoelastic solution. If the applied voltage is higher, the greater field strength will cause the jet to accelerate faster, and a greater volume of solution will be drawn from the tip of the needle. This may result in a smaller and less stable Taylor cone. When the drawing of the solution to the collection plate is faster than the supply from the source, the Taylor cone may recede into the needle. In most cases, a higher

voltage will lead to a greater stretching of the solution due to the greater columbic forces in the jet as well as the stronger electric field. These have the effect of reducing the diameter of the fibers and also encourage faster solvent evaporation. At a higher voltage, it has been found that there is a greater tendency for bead formation (Dietzel, et al. 2001). It was also reported that the shape of the beads changes from spindle-like to spherical-like with increasing voltage (Zhong, et al. 2002). Given the increased stretching of the jet due to higher voltage, there should be less bead formation (Jarusuwannapoom, et al. 2005). The increase in bead density due to increase in voltage may be the result of increased instability of the jet as the Taylor cone recedes into the syringe needle (Zhong, et al. 2002). Increasing voltage will increase the bead density, which at an even higher voltage beads join together to form a thicker diameter fiber.

2.4.2.2 Solution Feed Rate

Solution feed rate determines the amount of solution available for electrospinning. For a given voltage, there is a corresponding feed rate if a stable Taylor cone is to be maintained. When the feed rate is increased, there is an increase in the fiber diameter or bead size. This is apparent, as there is a greater volume of solution that is drawn away from the needle tip (Zhong, et al. 2002). A lower feed rate is more desirable, as the solvent will have more time for evaporation (Yuan, et al. 2004).

However, there is a limit to the increase in the diameter of the fiber due to higher feed rate. If the feed rate is at the same rate at which the solution is carried away by the jet, there must be a corresponding increase in charges when the feed rate is increased. Thus there is a corresponding increase in the stretching of the solution, which counters the increased diameter due to increased volume. Due to the greater volume of solution drawn from the tip, the jet will take a longer time to dry. As a result, the solvents in the deposited fibers may not have enough time to evaporate given the same flight time. The residual solvent causes the fibers to fuse together where they

make contact forming webs. This is advantageous in applications such as SOFCs where high surface area is desired.

2.4.2.3 Temperature

The temperature of the solution has both the effect of increasing its evaporation rate and reducing the viscosity of the polymer solution. Demir et al. (2002) observed that when polyurethane was electrospun at a higher temperature, the fibers produced had a more uniform diameter. This may be due to the lower viscosity of the solution and greater solubility of the polymer in the solvent that allows even more stretching of the solution. With a lower viscosity, the electrostatic forces are able to exert a greater stretching force on the solution, thus resulting in fibers of smaller diameter. Increased polymer molecule mobility due to increased temperature also allows the electrostatic force to stretch the solution further.

2.4.2.4 Effect of Collector Material

To initiate an electrospinning process, an electric field must be present between the source and the collector. So for this reason, most of the collectors in an electrospinning process are made out of a conductive material such as aluminum foil, which is electrically grounded so that there is a stable potential difference between the source and the collector. In the case when a non-conducting material is used as a collector, charges on the electrospinning jet will quickly accumulate on the collector, which will result in fewer fibers deposited. Fibers that are collected on the non-conducting material usually have a lower packing density compared with those collected on a conducting surface. The repulsive forces of the accumulated charges on the collector cause this phenomenon.

For a non-conducting collector, the accumulation of the charges may result in the formation of 3D fiber structures due to the repulsive forces of the like-charges. However, even for conductive collectors, when the deposition rate is high and the fiber mesh becomes thick enough, there will

also be a high accumulation of residual charges on the fiber mesh since polymer nanofibers are generally non-conductive. This may result in the formation of dimples on the fiber mesh.

The porosity of the collector seems to have an effect on the deposited fibers. Experiments with porous collectors such as paper and metal mesh have shown that the fiber mesh collected had a lower packing density than smooth surfaces such as metal foils (Seeram , et al. 2005). This can be attributed to the diffusion and rate of evaporation of the residual solvents on the fibers collected. In a porous target, there is faster evaporation of residual fibers due to higher surface area while smooth surfaces may cause an accumulation of solvents around the fibers due to slow evaporation rate. Due to the wicking and diffusion of the residual solvents on the fibers, the fibers may be pulled together to give a more densely packed structure.

Whether or not the collector is static or moving also has an effect on the electrospinning process. While rotating collectors have been used to collect aligned fibers, they were also found to assist in yielding fibers that are dry. This is useful because certain solvents such as di-methyl form-amide (DMF), which are good for electrospinning but have a high boiling point, may result in wet fibers during collection. A rotating collector will give the solvent more time to evaporate and also increase the rate of evaporation of the solvents on the fibers. This will improve the morphology of the fiber where distinct fibers are required.

2.4.2.5 Diameter of Needle Orifice

The internal diameter of the electrospinning needle will have some effect on the electrospinning process. A smaller internal diameter will reduce the clogging as well as the amount of beads in the electrospun fiber (Mo, et al. 2004). The reduction in the clogging could be due to the lower degree of exposure of the unspun solution to the atmosphere. Reduction in internal diameter of the needle will reduce the diameter of the electrospun fibers. When the size of the droplet at the tip of the orifice is decreased, such as in the case of a smaller internal diameter of the orifice, the

surface tension of the droplet increases. For the same voltage supplied, a greater columbic force is required to cause jet initiation. As a result, the acceleration of the jet decreases and allows more time for the spun solution to be stretched and elongated before it is collected. However, if the diameter of the orifice is too small, it may not be possible to electrospin a droplet of solution at the tip of the orifice.

2.4.2.6 Offset Distance Between the Tip and Collector

In most electrospinning scenarios, the flight time as well as the electric field strength will affect the electrospinning process and the resultant fibers. When the distance between the tip and the collector is altered, it has a direct effect on both the electric field strength and the flight time. For independent fibers to form, the electrospinning jet must be allowed time for most of the solvents to be evaporated. When the distance between the tip and the collector is reduced, the jet will have a shorter distance to travel before it reaches the collector plate. Moreover, the electric field strength will also increase at the same time, thus increasing the acceleration of the jet. As a result, there may not be enough time for the solvent to evaporate. When the distance is too low, excess solvent may cause the fibers to merge where they contact to form junctions resulting in inter and intra layer bonding. This interconnected fiber mesh may provide additional strength to the resultant scaffold.

Depending on the solution property, the effect of varying the distance may or may not have a significant effect on the fiber morphology. In some cases, changing the distance may not have significant effect on the diameter of the fibers. It is also observed that more beads are formed when the distance was too low (Xia, et al. 2003). The formation of beads may be due to the result of the increased field strength between the needle tip and the collector. Decreasing the distance will have the same effect as increasing the voltage supplied and this will cause an increase in the field strength. As mentioned earlier, if the field strength is too high, the increased instability of

the jet may encourage bead formation. However, if the distance is such that there is optimal electric potential, then there will be fewer beads formed.

2.4.3 Environmental Parameters

The effect of the atmosphere surrounding the electrospinning jet is one of the areas that is poorly investigated. Any interaction of the jet with the surroundings will have an effect on the diameter and the morphology of the fibers formed.

2.4.3.1 Humidity

Environmental humidity may have an effect on the electrospinning solution. At high relative humidity, water may condense on the surfaces of the fibers during electrospinning. This may influence the fiber morphology. For instance, Casper et al. (2004) observed that an increase in the humidity during electrospinning caused circular pores to form on the fiber surfaces. High humidity also lead to the fabrication of fibers with a thicker diameter.

2.4.3.2 Type of Atmosphere

The composition of the gas in the electrospinning chamber will have an effect on the process. Each gas type behaves differently under high electrostatic fields. For example, helium can break down under high electrostatic field, thus making electrospinning impossible (Baumgarten 1971). However, Baumgarden (1971) found that when a gas with higher breakdown voltage was used (e.g. Freon – 12), the fibers obtained were twice the diameter of those electrospun in air given all other conditions equal.

2.4.3.3 Pressure

It is possible to investigate the effect of pressure on the electrospinning jet. Generally, a reduction in the pressure surrounding the electrospinning jet does not improve the electrospinning process.

When the pressure is below atmospheric pressure, the polymer solution in the syringe will have a greater tendency to exhibit unstable flow out of the needle (Seeram , et al. 2005). As the pressure decreases, rapid bubbling of the solution occurs at the needle tip. At a very low pressure, electrospinning is not possible due to direct electrical discharge (sparking) between the needle and collector.

Chapter 3

Methods and Materials

3.1 Experimental Setup

Three different molecular weights of Mowiol (Synthetic Polyvinyl alcohol (PVA)) purchased from Sigma-Aldrich (MW_1 = 9,000 – 10,000, 80% hydrolyzed; MW_2 = 13,000 – 23,000, 98% hydrolyzed and MW_3 = 31,000 – 50,000, 87%-89% hydrolyzed) were used as a polymer source without any modifications. The three molecular weights were selected in such a way that they represented low molecular weight, medium molecular weight and high molecular weight polymers as specified in the literature. PVA was selected because it is easily soluble in distilled water when compared to other polymers. The percentage of hydrolyzation also affects the ability of the polymers to dissolve in water. At lower hydrolyzation percentages, the polymers are more easily able to dissolve in water. Mowiol is suitable for this study as it can thermally decompose at temperatures below 200 $^{\circ}$C.

Cerium nitrate hexahydrate ($Ce(NO_3)_3 \cdot 6H_2O$) and nickel nitrate hexahydrate ($Ni(NO_3)_3.6H_2O$) purchased from Sigma-Aldrich were used as sources of ceria and nickel without any modifications. GDC solution (Li 308 – Aq. Gd:CeO_2 dispersion, dopant level: 22% Gd, 26.7 wt./wt.% of Gd:CeO_2) supplied by Cerion enterprise were used as a source of cerium in preliminary studies. Distilled water was used to dissolve the polymer and the ceramic nitrates.

A Barnstead Super-Nuova hot plate was used to heat the solutions. Magnetic stirring in the range of 50-1200 rpm was used. Speed and temperature were controlled in 1 rpm and 1°C increments.

A typical electrospinning system consists of a high voltage supply, a syringe pump, a collector, and a syringe. An electrospinning system that meets these requirements was built in the Earl. W. Brinkman Machine Tools Laboratory at RIT for this research.

In order to have a high electrical potential between the substrate and the needle tip, a Trek Model 610E high voltage power amplifier was used. This device can supply voltages up to 10 kV. As a high-voltage reference supply, a front panel dial commands the output voltage. The positive supply lead was connected to the stainless steel syringe tip with an alligator clip. The negative supply lead was connected to the base plate collector.

A New Era Model NE-1000 programmable single syringe pump was used to dispense the electrospinning solution at the desired feed rate. This pump can hold up to 60 cc syringe barrels. One can set a single pumping rate or set a dispensing volume. The infusion rate depends on the syringe used. The diameter of the syringe should be given before setting up the pumping rate or the dispensing volume. A flow rate as low as 0.73 µL/hour can be achieved using a 1 cc syringe barrel. A flow rate as high as 2100 ml/hour can be achieved using a 60 cc syringe barrel. This pump is fully programmable and operates stand-alone or from a computer. The syringe pump can infuse as well as withdraw. The NE-1000 has a stated dispensing accuracy of +/-1%. For this study, 5cc syringes were used with 20 gauge luer-lock (0.7 mm orifice diameter) stainless steel syringe tips. Any conducting material can be used as a collector. For purposes of this study, aluminum foil attached to a grounded metal plate was used as a collector.

After electrospinning was completed, an Across International Model VO-16020 vacuum oven was used for drying electrospun fibers on the aluminum foil substrate. This particular model is specifically designed for a very steady heating rate and optimal accuracy at temperatures up to 250 $^{\circ}$C with +/- 1 $^{\circ}$C accuracy. Once the fibers were dry enough, they were peeled away with small tongs.

A KSL-1600X high temperature muffle furnace was used to sinter the samples at high temperatures. The furnace consists of high quality alumina fiber insulation and 1800 ℃ grade $MoSi_2$ heating elements. It is controlled by high precision SCR (silicon controlled rectifier) universal power controller and temperature controller with a stated accuracy of +/-1 $^{\circ}$C.

SEM imaging was conducted using a Jeol JSM 6400 scanning electron microscope at the Chester F. Carlson Center for Imaging Science at RIT. SEM is a method for high resolution imaging of surfaces. An incident electron bean is scanned across the sample's surface, and the resulting electrons emitted from the sample are attracted and collected by a detector and translated into a signal. Imaging in a SEM can be done using secondary electrons to obtain fine surface topographical features or with backscattered electrons that give contrast based on atomic number. The Jeol JSM-6400 SEM is configured with a Noran energy dispersive X-ray analyzer (EDS system). The EDS analysis system enables the SEM to perform compositional analysis on specimens. Samples were prepared by sputter coating the polymer-ceramic nanofiber mat with gold and palladium. An SPI-module sputter coater was used for coating the polymer-ceramic nanofiber mats with gold.

Diffraction patters were acquired using a D/MAX-IIB Rigaku powder X-Ray diffractometer in the Department of Mechanical Engineering at Rochester Institute of Technology (RIT).

3.2 Experimental Methodology

Fabrication of ceramic nanofibers by electrospinning is a three-step process. In the first step, a solution needs to be prepared. In the second step, fibers need to be electrospun and peeled from the substrate. In the final step, the polymers present in the fibers need to be burned out, and the ceramic particles need to be sintered without compromising the morphology of the fibers.

3.2.1 Ink Preparation

Composite ceramic-polymer solution was prepared by mixing ceramic nitrates with a polymer solution. Except for the preliminary experiments, all the experiments were carried out using Mowiol as a polymer, cerium nitrate hexahydrate and nickel nitrate hexahydrate as a source of nickel and cerium, and distilled water. Preliminary experiments were conducted by mixing GDC (by Cerion enterprise) with Mowiol solution. Predetermined quantities of polymer solution and ceramic were measured and mixed to form a ceramic-polymer solution. The procedure used to find the working range of the polymer concentration and the ceramic concentration is given in Chapter 4 of this study. A Barnstead Super-Nuova hot plate stirrer was used to mix the solutions together. When heating up the solution and stirring it, the beaker was kept closed using aluminum foil to minimize the loss of water vapor. Once mixed, the solution was transferred to a 5cc syringe for electrospinning. Unused solution was typically stored in a 35ml mixing cup and remixed using a Thinky ARE-310 planetary centrifugal mixer prior to subsequent use. The spinning of the ink in a centrifugal mixer causes the mixture to heat up, thus reducing the viscosity of the polymer solution. This heating effect made the transfer into the 5cc syringe easier.

Since materials used for this solution have a high cost, and a large quantities of solution are required for accurate and repeatable viscosity measurements, the solid loading fractions of the solutions were used in place of viscosity, viz. the ratio of the mass of ceramic and polymer (in grams) to the volume of distilled water.

3.2.2 Electrospinning and Peeling

Each 5cc syringe with a 20G syringe tip was filled with a ceramic-Mowiol solution and loaded into the NE-1000 programmable syringe pump. The stainless steel syringe tips were connected to the positive terminal of the Trek Model 610E high voltage power supply. An aluminum sheet was

placed on the grounded mild steel plate, and adhesive tape was used to keep it in place. The distance between the syringe tip and the collector was set at a predetermined position. The feed rate of the pump was set at a predetermined value, and the potential between the syringe tip and the collector was increased slowly until it reached the predetermined value. The distance between the collector and the syringe tip, the voltage, and the syringe pump feed rate were fine-tuned based on the quality of electrospinning observed. Figure 7 shows the electrospinning setup in the Earl W. Brinkman lab at RIT.

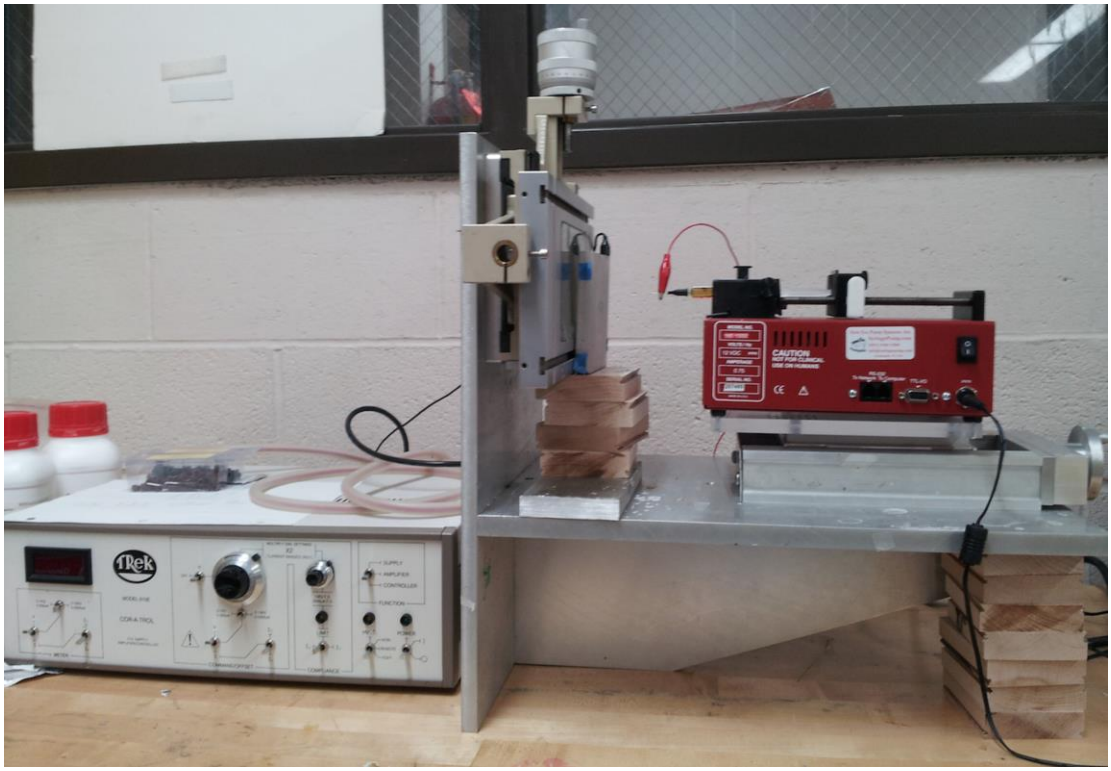

Figure 7: Electrospinning setup in Earl W. Brinkman lab

Once the fibers were deposited on the aluminum foil, the foil was placed in the vacuum oven set at the prescribed temperature. After the desired amount of time, the foil was taken out of the vacuum oven and the fibers were peeled away with small tongs.

3.2.3 Post Processing Conditions

Once the fibers were peeled from the substrate, they were placed in a ceramic bowl and sintered in the KSL-1600X high temperature muffle furnace for a predetermined time and temperature. The temperatures were selected in such a way that the polymer matrix decomposed while allowing the ceramic nanofiber network to maintain its structural integrity. Following this calcining step, the material was carefully transferred over to the measuring/analysis apparatus.

3.2.4 Analysis

SEM images were captured to understand the fiber morphology. EDS data was captured to get an idea about the elemental compositions of the fibers. XRD data was collected to get the diffraction pattern and hence the crystallinity of the material. Different sets of samples were used to conduct this part of the experiment.

1. Jeol JSM 6400 Scanning Electron Microscope

Samples were sputter coated with gold using a SPI-sputter coater module and then transferred onto a conductive (graphite) adhesive tape placed on the SEM fixture. The SEM fixtures were then slowly loaded into the scanning electron microscope. The microscope was focused on an area with fibers and SEM images were captured. EDS analysis system coupled with the SEM captured the EDS data.

2. Rigaku DMax-IIB Powder Diffractometer

The Rigaku powder diffractometer was used for X-ray diffraction analysis data. Samples were powdered and mounted on glass slides and scanned over the full 2θ range at a scan rate of 2 seconds per step at intervals of 0.020°. X-ray diffraction provides a definitive structural information, interatomic distances, and bond angles. The output of the analysis is typically a

unique diffraction pattern. This diffraction pattern is then compared against the full International Center of Diffraction Data (ICDD) powder database for bulk mineral analysis. The output from the XRD central computer was stored in an MS Excel spreadsheet.

Chapter 4

Experimental Results and Discussion

4.1 Feasibility Tests

Initial experiments were conducted to test the feasibility of electrospinning with the electrospinning system setup in the lab. Polyvinyl alcohol (PVA) (Mw: 31,000 – 50,000) purchased from Sigma Aldrich was mixed in warm water at 55 °C and was electrospun. A voltage of 6,000 V, flow rate of 0.2 ml/hr, and a distance of 4 cm was used for this experiment. The as-spun fibers were then taken and analyzed in the SEM. It revealed that the setup was capable of electrospinning fibers with diameter of 50-70 nm as shown in Figure 8. The electrospinning setup employed a vertical shaft configuration, resulting in unwanted droplets visible in the SEM image. The orientation of the electrospinning setup was subsequently changed to the horizontal position to avoid these droplets.

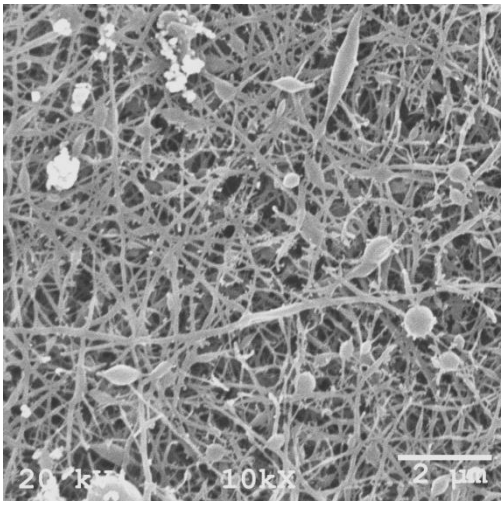

Figure 8: SEM image of as spun PVA nanofibers

Before preparing the ceramic-polymer solution required for this study, different molecular weight polymers were mixed with distilled water at different weight percentages and electrospun to understand the effect of molecular weight of Mowiol, weight percentages of Mowiol solution and

science behind electrospinning. Initially, low molecular weight polymer (MW_1 = 9,000 – 10,000, 80% hydrolyzed) was dissolved in water to form 10 wt./wt.% of polymer solution that was then electrospun. Due to the low molecular weight and low concentration of the polymer solution, electrospraying occurred instead of electrospinning. As the percentage of polymer was increased, beads with wet droplets were formed instead of fibers. Then medium molecular weight (MW_2 = 13,000-23,000; 98% hydrolyzed) polymer was dissolved in water and electrospun. Droplets were collected when the polymer concentration was low, and fibers with beads and droplets were formed when the polymer percentage was increased. Then high molecular weight (MW_3 = 31,000 – 50,000; 87%-89% hydrolyzed) polymer was dissolved in water and electrospun. When the polymer concentration was low (10%), beads were formed at times with low productivity. So the polymer concentration was increased slowly to 25 wt./wt.%, where thin, continuous nanofibers were formed without any issues (beads or droplets). As the weight percentage was further increased, the thick polymer solution eventually clogged the syringe tip.

Next, the ceramic-polymer solution was placed in a ceramic crucible and sintered at different temperature cycles. Initially the temperature was increased to 125 °C at a rate of 5 °C/min. and held at this temperature for about 2 hours. The temperature was then increased to 600 °C at a rate of 1 °C /min. The EDS data was captured for this sample. The EDS data showed that some of the polymer was still not burned out, so the temperature was increased to 250 °C and the test was run again. The EDS data captured this time showed that there was no carbon present in the sintered samples. Another way to determine the burning temperature of the polymer would be thermo gravimetric analysis (TGA).

In order to determine the amount of ceramic nitrate to be added to the polymer solution, a ceramic-polymer solution was prepared by adding 1gram of cerium nitrate hexahydrate to the 20 wt./wt.% of polymer solution. This solution was electrospun and then sintered. The sintered sample had a powder form instead of a fibrous structure. The amount of ceramic nitrates were

increased by 1gram every step, and the SEM images of sintered nanofibers were captured. The percentage of ceramic nitrates was increased until the SEM images revealed a fibrous structure in nanoscale. As the percentage of ceramic nitrates crossed a certain level, the quality of electrospinning deteriorated, and beads started to form on the collector. Ceria nitrate hexahydrate and nickel nitrate hexahydrate composite solutions were prepared with increasing concentrations, and the SEM images of sintered nanofibers were captured. The percentage of ceramic was increased until the SEM images revealed a fibrous structure.

The prepared solutions were transferred to the syringe mounted in a syringe pump. The feed rate of the pump was set in such a way that after a droplet at the syringe tip was cleaned using a Q-tip, a new droplet immediately formed at the tip of the syringe. Based on experience from previous experimentation, an offset distance of 3cm between the syringe tip and the collector was used. The voltage was slightly increased until a stable Taylor cone was observed,when seen through a Dyno-Lite microscope camera.

Once composite ceramic-polymer nanofibers were consistently formed. The temperature cycle was fine tuned to maintain the fibrous structure. After conducting a series of trials with different ramping temperatures (0.5 °C/min., 0.75 °C/min. and 1 °C/min.) and different hold times (1 hr, 1.5 hrs, 2hrs, 4 hrs and 6 hrs), it was determined that best results were obtained after ramping the temperature up to 250 °C at 0.5 ^{0}C/min., holding there for four hours, then ramping up to 800^{0}C at 1 °C/min. and holding there for 7-8 hours.

4.2 Ceramic-Polymer Solution Preparation

A 20 wt. % Mowiol solution was made by adding 6 grams of Mowiol to 25 ml of distilled water. First, the distilled water was heated to 98 °C in a covered beaker using a water bath maintained at

140 °C. Once the distilled water reached the desired temperature, Mowiol was slowly added and stirred at 500 rpm for 8 hours.

10 ml of this solution was then transferred into another closed beaker which was maintained at 98 °C using a water bath. 6 grams of cerium nitrate hexahydrate were slowly added to this solution and stirred at 300 rpm for a several hours until a uniform color consistency was achieved. The resulting solution was then ready for electrospinning.

Another 10 ml of the starting Mowiol solution was transferred into a closed beaker which was maintained at 140 °C using a water bath. 6 grams of nickel nitrate hexahydrate was slowly added to this solution and stirred at 500 rpm for several hours until a consistent color was achieved. The resulting nickel solution was then ready for electrospinning.

4.3 Electrospinning Ceramic-Polymer Solutions

The nickel-Mowiol and ceria-Mowiol solutions were loaded into 5cc syringes and were immediately used for electrospinning. Voltages of 7000V and 7800V were used, respectively, for cerium-based polymer solutions and nickel-based polymer solutions. The voltages were varied based on the observed quality of electrospinning. The distance between the syringe tip and the collector was maintained at 3cm. The solution feed rate was maintained at 0.3 ml/hour with the syringe pump. The voltage and the distance between the syringe tip and the collector were slightly varied based on the quality of the electrospun fibers. If intermittent sparks between the needle and aluminum substrate were observed, then the offset distance was increased or the voltage was reduced. If the force of the electric field was not high enough for electrospinning, then the voltage was slightly increased or the distance between the collector and the syringe tip was reduced. A mild steel plate covered with aluminum foil was used as the collector. Once the fibers were electrospun, the aluminum foil was peeled and dried in a vacuum oven maintained at

a temperature of 70 °C for about 6 hours. The nanonetwork mat was then peeled gently using a pair of small tongs. Figures 9 and 10 show the SEM images of as-spun ceria-Mowiol and nickel-Mowiol nanofibers respectively. As-spun ceria-Mowiol fibers had an average diameter of less than 190nm, and nickel-Mowiol fibers had an average diameter of less than 300nm.

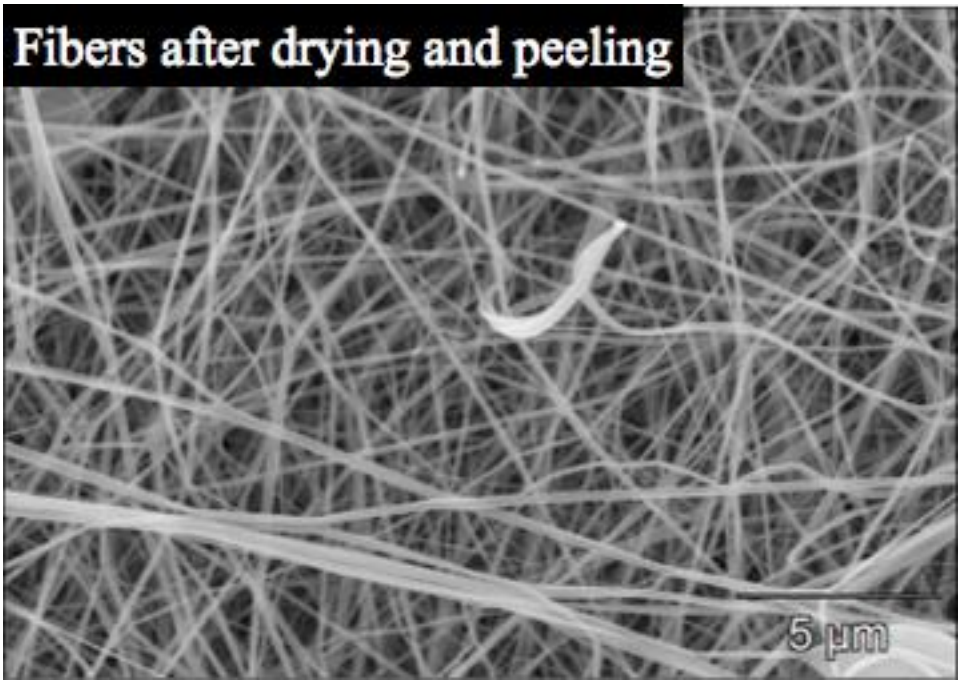

Figure 9: SEM image of as-spun ceria-Mowiol nanofibers

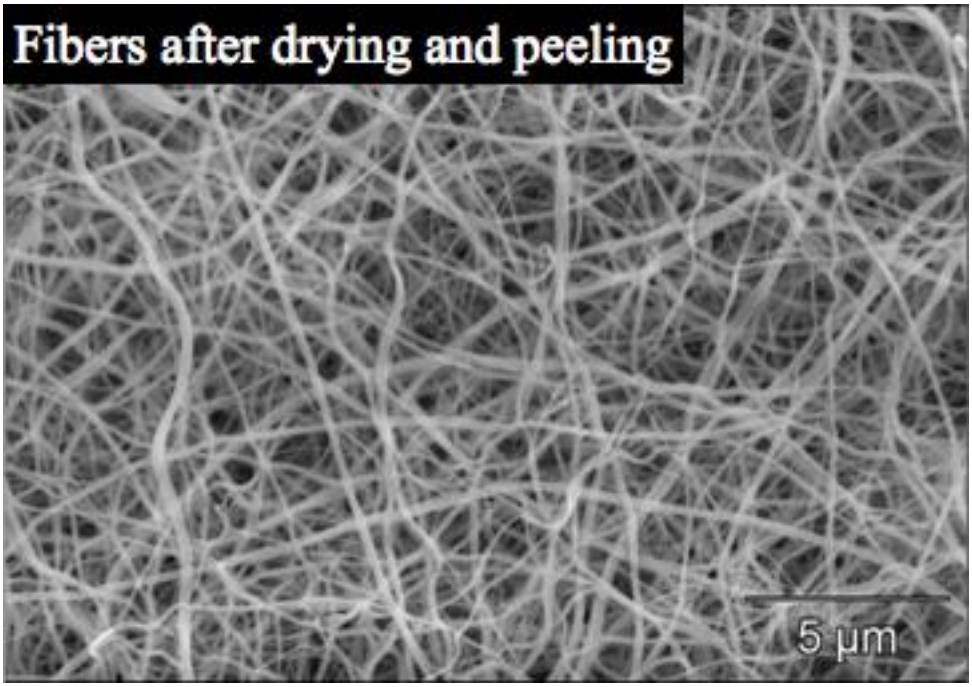

Figure 10: SEM image of as-spun nickel-Mowiol nanofibers

4.4 Post Processing Conditions

Once these fibers were peeled from the collector, they were calcined in the furnace at 800 °C. First, the temperature was increased to 250 °C at a rate of 0.5 °C/min. and held at that temperature for 4 hours to give the polymer enough time to burn out. The logic behind the slow ramping up is to burn out the polymer in the fibers so that the ceramic fibers have sufficient support before calcination.

After this initial step, the temperature was increased to 800 °C at a rate of 1 °C/min. It was held at this temperature for about 7 hours to give the ceramic nanoparticles enough time for calcination. The slow ramp speed was designed to calcine the polymer in the fibers very slowly so that the ceramic nanofibers would not disintegrate from a lack of structural support. The final firing schedule is given in Figure 11.

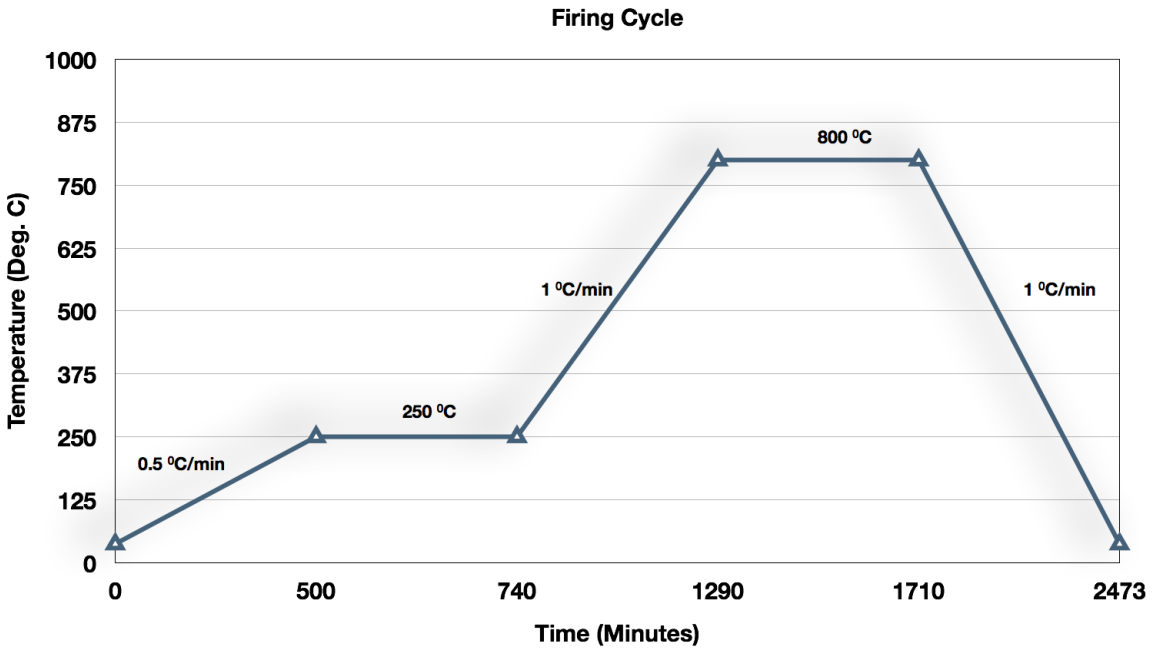

Figure 11: Firing schedule for ceramic-Mowiol composite nanofibers

Once the samples were calcined, they were then carefully taken to the measurement systems where the SEM images, EDS data and the XRD data were collected.

4.5 Results

4.5.1 SEM Images and EDS Data

Figures 12 and 13 show SEM images of ceria fibers and nickel oxide fibers. The average diameters of cerium oxide fibers are about 890 nm, while the diameters of nickel oxide fibers formed are on the order of 550 nm. At some stage during the calcination cycle, thin and long as-spun nanofibers change morphology into shorter nanofibers with a larger diameter. The as-spun nanofibers have both thin and thick filaments. It is hypothesized that below a certain diameter, particularly thin nanofibers do not have sufficient strength to withstand high calcination temperatures after decomposition of the organic components. The larger diameter nanofibers have sufficient green strength to withstand the high temperatures after the organic components have decomposed. It is hypothesized that these fibers shrink, or contract, during thermal processing.

From a given mass that has survived the temperature, thin long fibers would therefore contract to shorter fibers with larger diameters. This can be considered analogous to contraction of human muscle tissue. When the arm is in the extended state, the muscle is long and slender. When the arm is folded, it becomes short and thick.

Figure 14 shows the EDS spectra for as-spun ceria-Mowiol nanofibers. The spectra show a high carbon peak as well as several cerium peaks along with gold and palladium peaks. The carbon peak is due to the organic Mowiol PVA present in the as-spun fibers. The gold and palladium peaks are due to the sputter coating done using the SPI module.

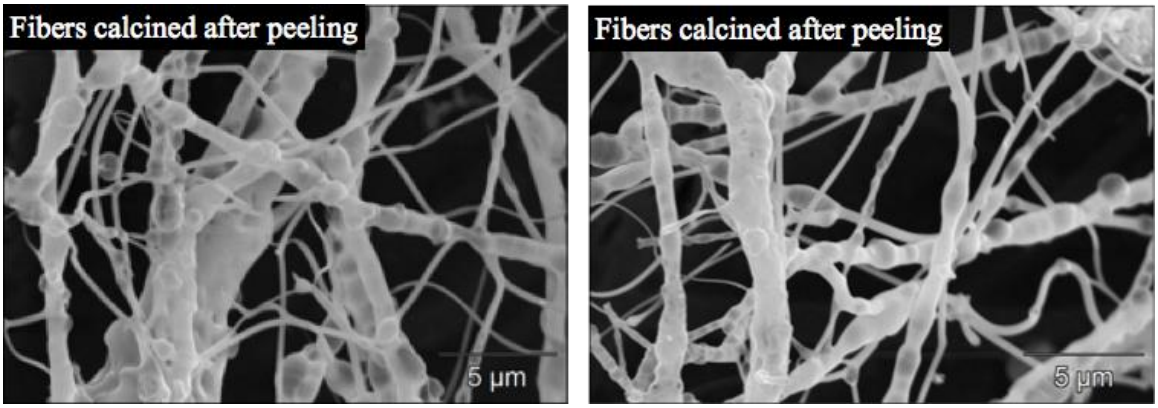

Figure 12: SEM images of cerium oxide nanofibers

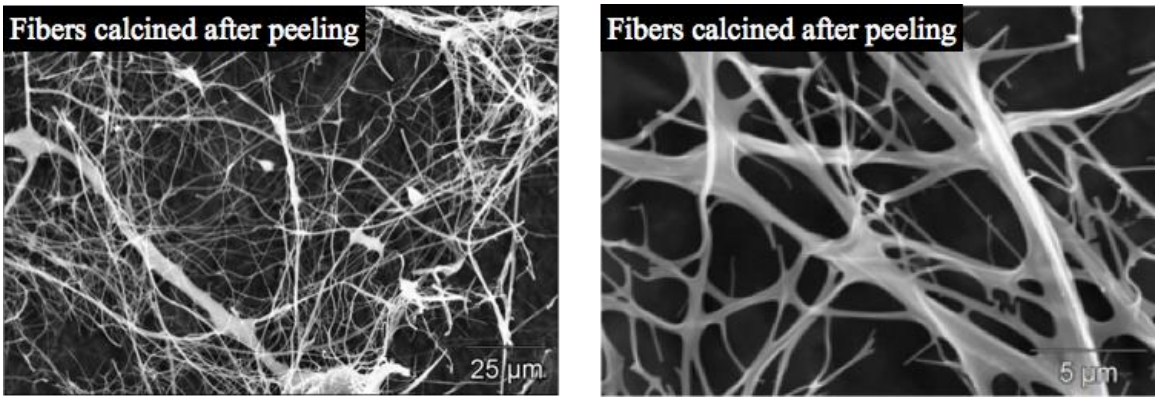

Figure 13: SEM images of nickel oxide nanofibers

Figure 15 shows the EDS data for calcined ceria nanofibers. The EDS data shows several peaks of cerium in its different phases. The small peak of carbon is due to the graphite tape used on the SEM fixture. The gold and palladium peaks are due to the sputter coating material. The oxygen peak also shows that CeO_2 is formed after sintering the nanofibers.

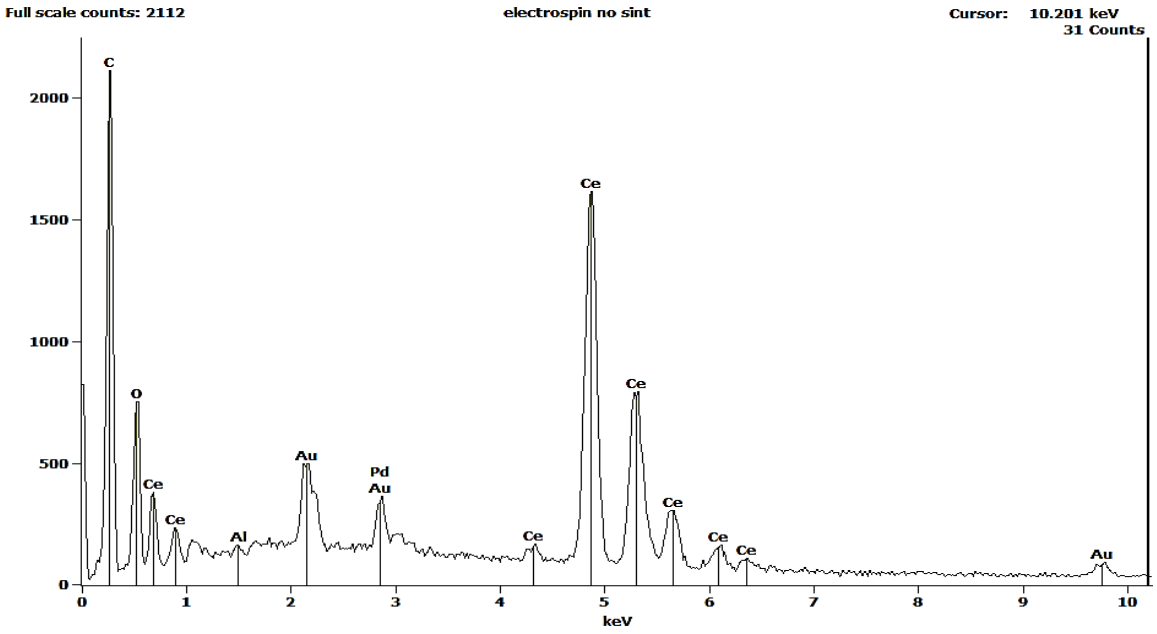

Figure 14: EDS spectra for as spun cerium-Mowiol nanofibers

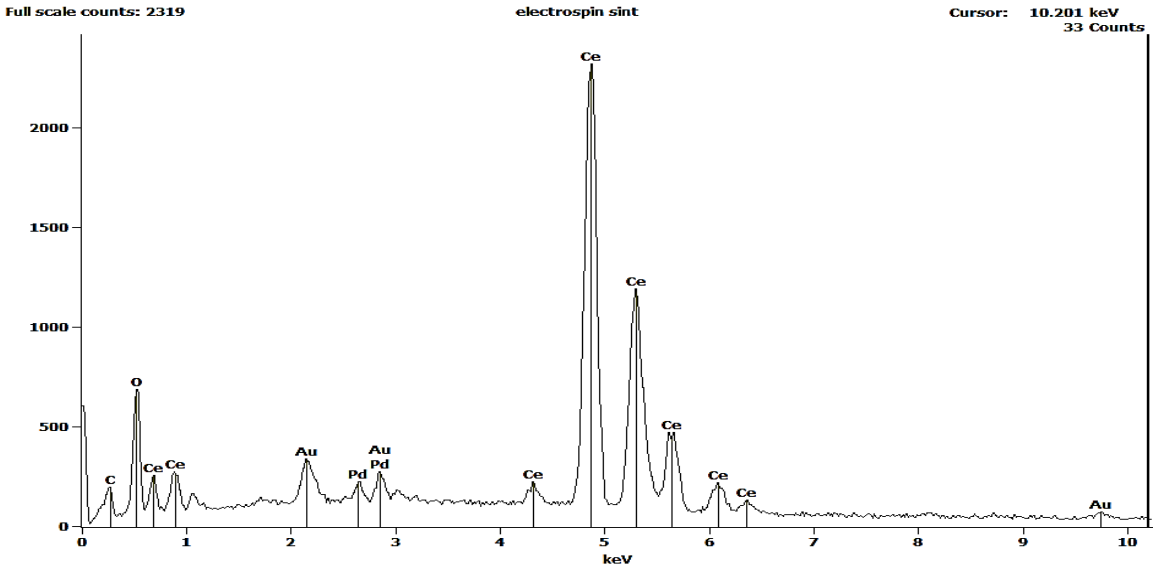

Figure 15: EDS spectra of sintered ceria nanofibers

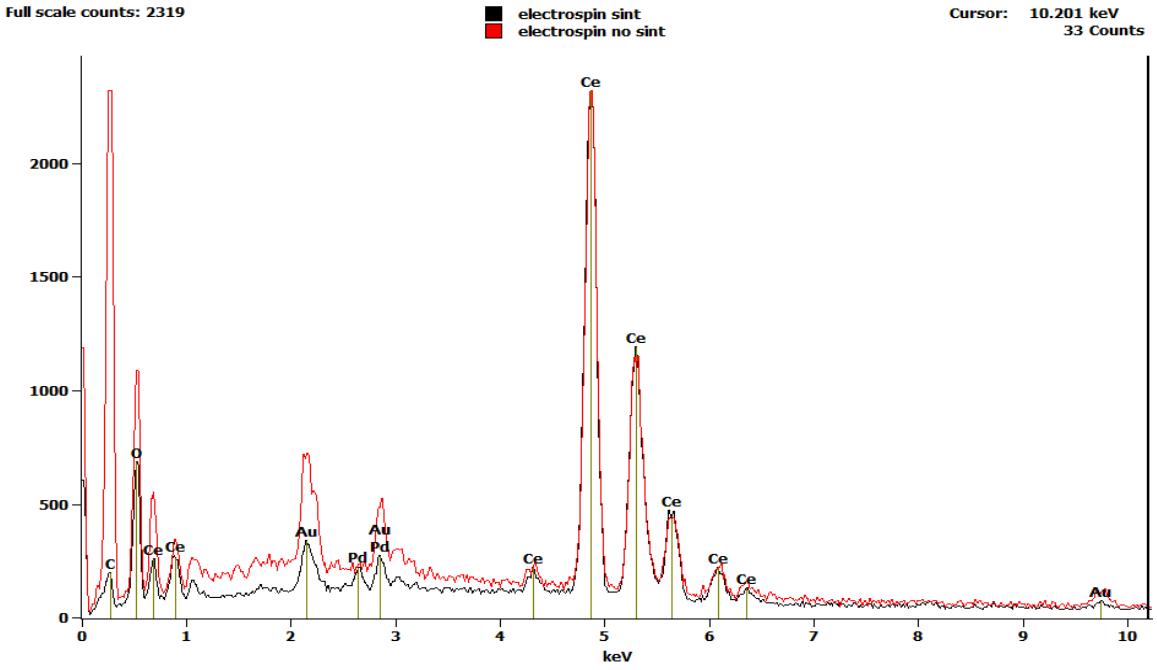

Figure 16: EDS spectra comparison of as spun and sintered ceria nanofibers

From the EDS comparison in Figure 16, it can be observed that the sintered samples have virtually no carbon present in them and are entirely made of ceria. There is a small carbon peak

present in the sintered sample EDS spectra, which is accounted for by the graphite tape used as the background.

Figure 17 shows EDS Spectra for sintered nickel oxide nanofibers. The EDS data shows three nickel peaks that represent nickel in three different phases. The small carbon peak is the result of the background graphite tape used on the SEM fixtures. This EDS spectra shows that nickel oxide fibers have been successfully synthesized.

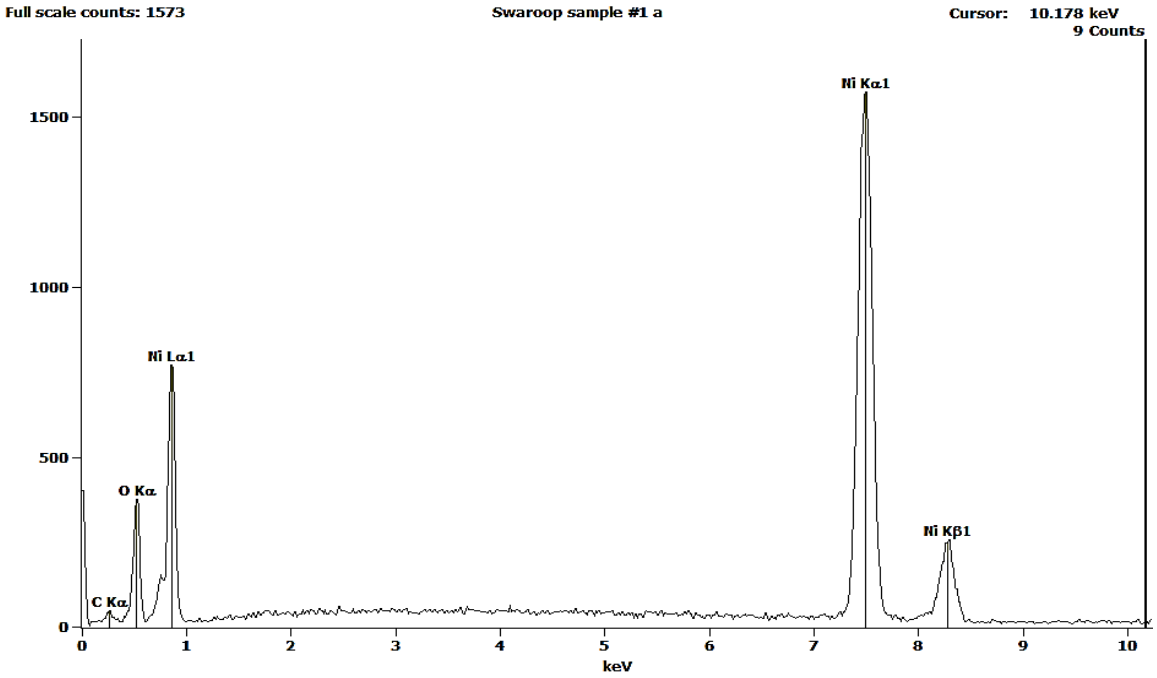

Figure 17: EDS spectra for sintered nickel nanofibers

4.5.2 XRD Analysis

4.5.2.1 Cerium oxide

The EDS data showed that only CeO_2 phases are present in the fibers, and this was further confirmed by XRD analysis. The XRD patterns of CeO_2 materials are shown in Figure 18 for the as-spun and sintered nanofibers at 700, 800 and 900 °C. It is noted that there are no crystal-phase peaks of CeO_2 in the XRD pattern of the as-spun nanofiber. This indicates that the fibers were

amorphous rather than crystalline at the time of electrospinning. A total of 16 peaks were observed for sintered samples. These peaks were compared to the catalogue and identified as CeO_2.

The CeO_2 XRD pattern was indexed using powder diffraction file (PDF) card number 00-034-0395 for cerium oxide. The cerium oxide in the library was prepared at NBS, Gaithersburg, MD, USA, by Dragoo, Domingues (1982) from co-precipitation of the oxides. The powder was calcined at 620 °C, formed into a billet without binder, isostatically pressed, and then hot-pressed in an alumina die for 30 minutes at 1350 °C with an applied stress of 28MPa. The color of the sample was light gray, yellowish brown.

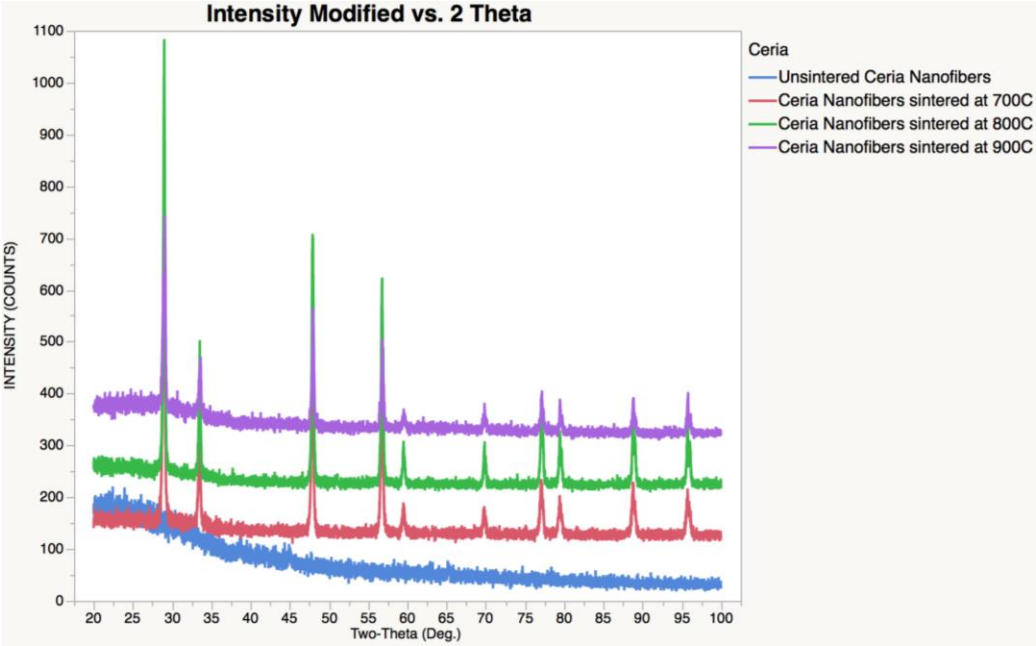

Figure 18: XRD data of as-spun and sintered ceria nanofibers

Cerium oxide fibers tested by XRD had a face centered cubic lattice structure with a=b=c=5.41134 A° and α=β=γ=90°. Table 2 shows the angles where the peaks are formed.

Table 2: Cerium oxide nanofibers XRD summary

#	d(A)	I(f)	h	k	l	2-Theta	Theta	1/(2d)
1	3.1234	100	1	1	1	28.555	14.277	0.1601
2	2.7056	30	2	0	0	33.082	16.541	0.1848
3	1.9134	52	2	2	0	47.479	23.739	0.2613
4	1.6318	42	3	1	1	56.335	28.167	0.3064
5	1.5622	8	2	2	2	59.086	29.543	0.3201
6	1.3531	8	4	0	0	69.401	34.701	0.3695
7	1.2415	14	3	3	1	76.699	38.350	0.4027
8	1.2101	8	4	2	0	79.069	39.535	0.4132
9	1.1048	14	4	2	2	88.412	44.206	0.4526
10	1.0415	11	5	1	1	95.396	47.698	0.4801
11	0.9566	4	4	4	0	107.264	53.632	0.522
12	0.9147	13	5	3	1	114.729	57.365	0.5466
13	0.9019	6	6	0	0	117.317	58.658	0.5544
14	0.8556	9	6	2	0	128.392	64.196	0.5844
15	0.8252	6	5	3	3	137.970	68.985	0.6059
16	0.8158	5	6	2	2	141.566	70.783	0.6129

It could also be seen that increases in the calcination temperature resulted in an increase in the intensity and sharpness of the peaks. This indicates that calcination crystallized the as-spun amorphous ceria (Fuentes and Baker 2009).

4.5.2.2 Nickel oxide

The EDS data shows that only NiO phases are present in the fibers, and this was further confirmed by XRD analysis. The XRD patterns of NiO materials are shown in Figure 19 for the as-spun and sintered nanofibers at 700, 800 and 900 °C. It is noted that there are no crystal-phase peaks of NiO in the XRD pattern of the as-spun nanofiber. This indicates that the as-spun fibers were amorphous. A total of 8 peaks are observed in Figure 19. These peaks were compared to the catalogue and are consistent with NiO.

The NiO XRD pattern was indexed using powder diffraction file (PDF) card number 00-047-1049 for nickel oxide. The nickel oxide in the library was obtained from J.T. Baker Chemical Corp. The sample was annealed for 72 hours at 1100 °C. The color of the sample was green.

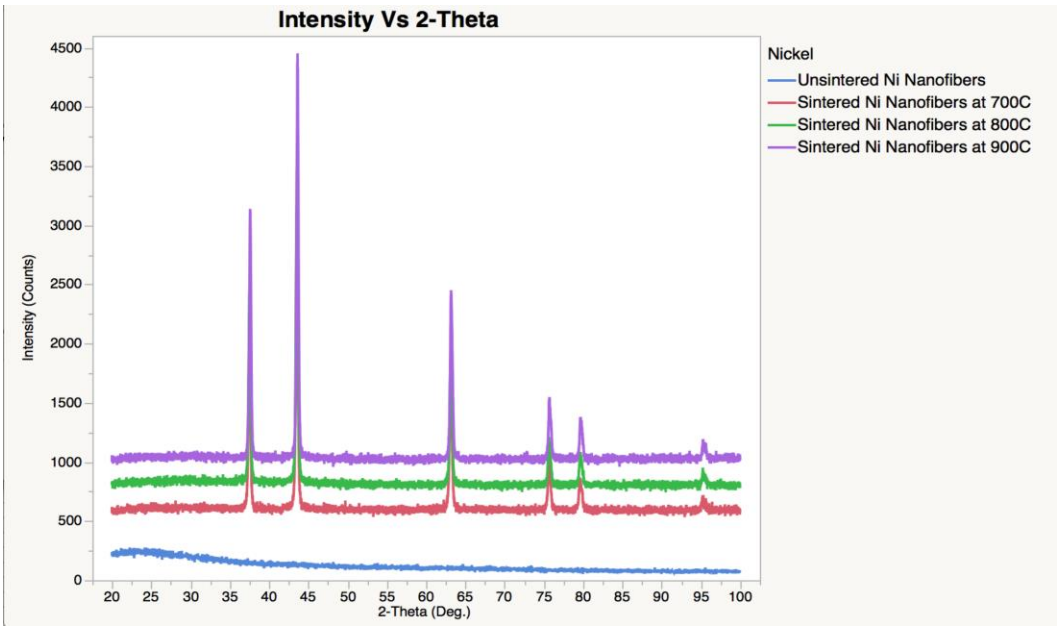

Figure 19: XRD analysis of as-spun and sintered nickel oxide nanofibers

Nickel oxide fibers tested by XRD were found to have a face centered cubic lattice structure with a=b=c=4.1771 A° and α=β=γ=90°. Table 3 shows the angles where the peaks are formed.

Table 3: Nickel oxide nanofibers XRD summary

#	d(A)	I(f)	h	k	l	2-Theta	Theta	1/(2d)
1	2.4120	61	1	1	1	37.248	18.624	0.2073
2	2.0890	100	2	0	0	43.276	21.638	0.2393
3	1.4678	35	2	2	0	62.879	31.439	0.3386
4	1.2594	13	3	1	1	75.416	37.708	0.3970
5	1.2058	8	2	2	2	79.408	39.704	0.4147
6	1.0443	4	4	0	0	95.058	47.529	0.4788
7	0.9583	3	3	3	1	106.992	53.496	0.5218
8	0.9340	7	4	2	0	111.122	55.561	0.5353

It could also be seen that progressively higher calcination temperature resulted in an increase in the intensity and sharpness of the peaks and hence crystallinity (Fuentes and Baker 2009) of the fibers.

Chapter 5

Conclusions and Recommendations

5.1 Summary

As mentioned in Section 1.5 of this study, the objective of this thesis was to develop a composite ceramic-polymer solution, to identify electrospinning conditions, and to develop post-processing procedures for the fabrication of continuous nanofiber networks of ceria and nickel by electrospinning. This study gives the method followed to identify the "sweet spots" for polymer concentration, ceramic loading fraction, electrospinning conditions and post processing parameters. An electrospinning system was set up using a single syringe pump, high voltage supply, and a mild steel plate covered with aluminum as a collector. An initial experiment was conducted to make sure that nanofibers could be electrospun using the setup. Next, a feasibility test was conducted to make sure that ceramic nanofibers were electrospun using the setup. Steps to prepare cerium-based and nickel-based polymer solutions were given in Section 4.2. Parameters such as voltage, feed rate etc., required to electrospin were given in Section 4.3. The post-processing conditions needed for the synthesis of ceramic nanofibers were given in Section 4.4. SEM images and EDS data presented in Section 4.5.1 showed that the calcined nanofibers did not have any residual organic material. The XRD data in Section 4.5.2 indicated that the calcined ceramic fibers are crystalline in nature.

Mowiol-$Ce(NO_3)_3$ and Mowiol-$Ni(NO_3)_3$ composite nanofibers were successfully fabricated using the electrospinning technique. Ceria and nickel oxide nanofibers were successfully synthesized by calcining the composite fibers at 800^0C for 8 hours. Morphology of both cerium-mowiol and nickel-mowiol composite nanofibers was smooth and became coarse after calcination. Diameter

of as spun nanofibers was smaller than the diameter of sintered ceramic nanofibers. Composite nanofibers were amorphous in structure, whereas sintered fibers were cubic in structure with space group when calcination temperature was 700-900^{0}C.

5.2 Contributions

Ceria and nickel oxide nanofibers are technologically important functional materials for many applications. The work described in this thesis contributes to the fabrication of these fibers. At the time of writing, there are few instances where ceria and nickel oxide nanofibers were fabricated. In all of those instances, the voltage applied was typically very high (around 10-15kV), and calcination took place on the glass collector itself. This thesis gives a method to peel the fibers from the collector and sinter it. Typically when a glass collector is used, the rate of deposition is drastically reduced as the amount of charge accumulated on the collector reduces.

The work described in this thesis contributes towards many applications ranging from fabrication of solid oxide fuel cells (SOFC's) to supercapacitors. Conventional SOFC's employ nickel-based cermet anodes, which exhibit good compatibility with electrolytes composed of stabilized zirconia or doped ceria. Nickel along with electrolyte ceramic material is commonly used as an anode material in solid oxide fuel cells. The fabrication techniques used for the fabrication of ceria can be replicated to produce gadolinium doped ceria (GDC) nanofiber networks. The methodology presented in this thesis can also be applied to fabricate several other ceramic nanofibers.

5.3 Future Recommendations

Triple phase boundary in SOFC's is defined as the boundary where the electrolyte, electrode and gases of solid oxide fuel cell come in contact. Material used as electrodes and electrolyte are

generally expensive, and the ability to create large triple phase boundary with the least possible amount of material would play a major role in reducing the prices of solid oxide fuel cells.

If continuous nickel and electrolyte nanofiber networks could be electrospun side-by-side, then the resulting triple phase boundary would be extremely large while using a minimal amount of anode and cathode materials.

Preliminary experiments have been conducted to explore the feasibility of parallel or side-by-side electrospinning. The electrospinning process was modified using dual material feeds so that the syringe tip was off center as shown in Figure 20. If solution A is placed in one of the syringes, and solution B is placed in the other syringe, then the two liquid feeds come out side-by-side. If it is made sure that there exists a single Taylor cone, then the resultant electrospun fibers would have a side-by-side morphology (fibers with material"A"- material "B").

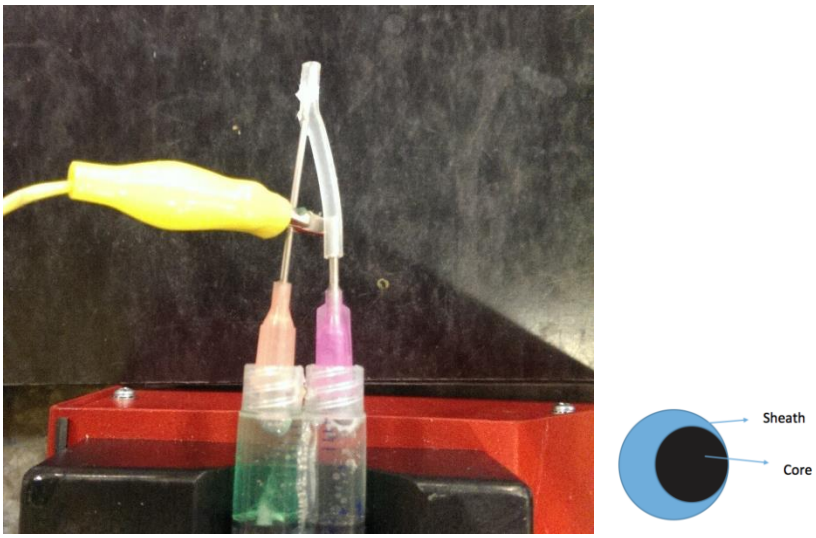

Figure 20: Method to fabricate parallel or side-by-side fibers by electrospinning

Figure 21: Novel method to fabricate parallel or side-by-side nanofibers

Figure 21 shows an alternative method to fabricate parallel or side-by-side nanofibers. In this approach, two different solutions are pumped into a chamber via two orifices. The design of the chamber is as shown in Figure 22. The two solutions are kept in different chambers until the instant they enter the syringe tip. The flow of liquid in the syringe tip should be predominantly laminar. When the viscosity of the two solutions are similar, then the output from the syringe tip should be a single Taylor cone with one half of one solution and the other half of the second solution.

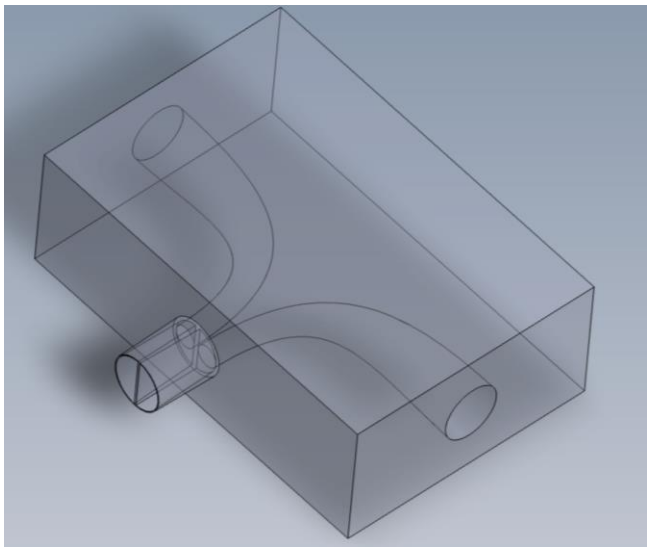

Figure 22: Chamber design

Yet another method that can be used to achieve a single Taylor cone from two feed streams is to join two long syringe tips with an alligator clip as shown in Figure 23. Once control is achieved

over parallel electrospun fibers, the next step would be to investigate electrospinning anode-electrolyte material and electrolyte-cathode materials. Side by side electrospun nanofibers have a potential to have long triple phase boundary with a unit amount of material.

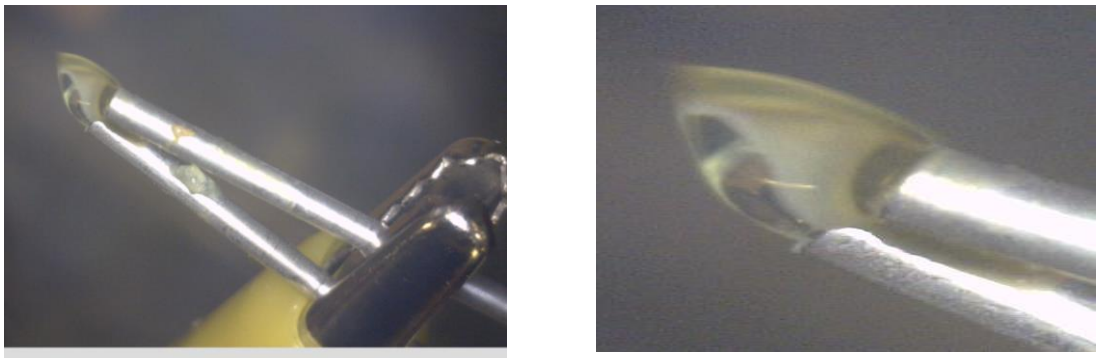

(a) (b)

Figure 23: (a) Single Taylor cone achieved by joining two syringe tips using an alligator clip; (b) close-up view

Bibliography

Baumgarten, Peter K. "Electrostatic spinning of Acrylic Microfibers." *Journal of Colloid Interface Science* (Elsevier) 36, no. 1 (May 1971): 71-79.

Bleiwas, Donald I. *Potential for Recovery of Cerium Contained in Automotive Catalytic Converters.* Open-File, U.S. Geological Survey, 2013, 10.

Bognitzki, M., et al. "Polymer, Metal, and Hybrid Nano- and Mesotubes by Coating Degradable Polymer Template Fibers (TUFT Process)." *Advanced Materials* 12, no. 9 (May 2000): 637-640.

Bullitt, E, G Gerig, S.M Pizer, Lin Weili, and S.R Aylward. "Measuring tortuosity of the intracerebral vasculature from MRA images." *IEEE Transaction of Medical Imaging* 22, no. 9 (September 2003): 1163-1171.

Carman, P.C. "Fluid flow through granular beds." *Transactions, Institution of Chemical Engineers*, no. 15 (1937): 150-166.

Casper, C L, J S Stephens, N G Tassi, D B Chase, and J F Rabolt. "Controlling surface morphology of electrospun polystyrene fibers: Effect of humidity and molecular weight in the electrospinning process." *Macromolecules* 37, no. 2 (2004): 573-578.

Choi, J.S, et al. "Effect of organosoluble salts on the nanofibrous structure of electrospun poly(3-hydroxybutyrate-co-3-hydroxyvalerate)." *International Journal of Biological Macromolecules* 34, no. 4 (August 2004): 249-256.

Chunwen, Sun, et al. "Mesoscale Organization of Nearly Monodisperse Flowerlike Ceria Microspheres." *The Journal of Physical Chemistry* 110, no. 27 (2006): 13445-13452.

Cooley, John F. Apparatus for electrically dispersing fluids. USA Patent US 692631 A. February 4, 1902.

Cuiru, Yang, Jia Zhidong, Xu Zhihai, Wang Ke, Guan Zhicheng, and Wang Liming. "Comparisons of fibers properties between vertical and horizontal type electrospinning systems." *Annual report conference on electrical insulation and dielectric phenomena.* Virginia Beach, VA: IEEE, 2009. 204-207.

Demir, M.M, I Yilgor, E Yilgor, and B Erman. "Electrospinning of polyurethane fibers." *The International Journal for the Science and Technology of Polymers* (Elsevier) 43, no. 11 (May 2002): 3303-3309.

Dietzel, J.M, J Kleinmeyer, D Harris, and N.C.B Tan. "The effect of processing variables on the morphology of electrospun nanofibers and textiles." *The International Journal for the Science and Technology of Polymers* 42, no. 1 (January 2001): 261-272.

Eda, Goki, and Satya Shivkumar. "Bead-to-fiber transition in electrospun polystyrene." *Journal of applied polymer sciences* 106, no. 1 (June 2007): 475-487.

Feng, J J. "The stretching of an electrified non-Newtonian jet: A model for electrospinning." *Physics of Fluids* (AIP) 14, no. 11 (November 2002): 3912-3926.

Feyman, Richard. *American Physical Society Meeting.* Caltech, December 29, 1959.

Fong, Hao, Weidong Liu, Chyi-Shan Wang, and Richard A Vaia. "Generation of electrospun fibers of nylong 6 and nylon 6-montmorillonite nanocomposite,." *The International Journal for the Science and Technology of Polymers* (Elsevier) 43, no. 3 (February 2002): 775-780.

Formhals, Anton. Artificial thread and method of producing same. US Patent US 2187306 A. January 16, 1940.

Formhals, Anton. Artificial thread and method of producing same. US Patent US 2187306 A. January 16, 1940.

Formhals, Anton. Process and apparatus for preparing artificial threads. US Patent Patent US 1975504 A. Ocotober 2, 1934.

Fuentes, Rodolfo O., and Richard T. Baker. "Structural, morphological and electrical properties of GdCeO prepared by citrate complexation method." *Journal of Power Sources* 186, no. 22 (January 2009): 268-277.

G.Taylor. "Disintegration of Water Drops in an Electric Field." *Proceedings of the Royal Society of London, Series A: Mathematical and Physical and Sciences* (The Royal Society) 280, no. 1382 (February 1964): 383-397.

Gorte, R J, S Park, J M Vohs, and C Wang. "Anodes for direct oxidation of dry hydrocarbons in a solid-oxide fuel cell." *Advanced Materials* 12, no. 19 (October 2000): 1465-1469.

Gostovic, D, J.R Smith, D.P Kundinger, K.S Jones, and E.D Wachsman. "Three-Dimensional Reconstruction of Porous LSCF Cathodes." *Electrochemical and Solid State Letters* (The Electrochemical Society) 10, no. 12 (2007): B214-B217.

Holtappels, P, C Sorof, M.C Verbraeken, S Rambert, and U Vogt. "Preparation of Porosity-Graded SOFC Anode Substrates." *Fuel Cells* 6, no. 2 (April 2006): 113-116.

Hou, H.Q, Z Jun, A Reuning, A Schaper, J.H Wendorff, and A Greiner. "Poly(p-xylene) nanotubes by coating and removal of ultrathin polymer template fibers." *Macromolecules* 35, no. 7 (February 2002): 2429-2431.

Huang, Z.M, Y.Z Zhang, S Ramakrishna, and C.T Lim. "Electrospinning and mechanical characterization of gelatin nanofibers." *The International Journal for the Science and Technology of Polymers* (Elsevier) 45, no. 15 (July 2004): 5361-5368.

Jarusuwannapoom, T, et al. "Effect of solvents on electro-spinnability of polystyrene solutions and morphological appearance of resulting electrospun polystyrene fibers." *European Polymer Journal* (Elsevier) 41, no. 3 (March 2005): 409-421.

Jin, H.J, S.V Fridrikh, G.C Rutledge, and D.I Kaplan. "Electrospinning Bombyx mori silk with poly(ethylene oxide)." *Biomacromolecules* 3, no. 6 (August 2002): 1233-1239.

Kim, J.W., A.V. Virkar, K.Z. Fung, K. Mehta, and S.C. Singhal. "Polarization Effects in Intermediate Temperature, Anode-Supported Solid Oxide Fuel Cells." *Journal of Electrochemical Society* 146, no. 1 (1999): 69-78.

Koombhongse, S, W Liu, and D.H Reneker. "Flat polymer ribbons and other shapes by electrospinning." *Journal of Ploymer Science; Part B: Polymer Physics* 39, no. 21 (September 2001): 2598-2606.

Koski, A, K Yim, and S Shivkumar. "Effect of molecular weight on fibrous PVA produced by electrospinning." *Materials Letters* 58, no. 3-4 (January 2004): 493-497.

Leach, Michelle K., Feng Zhang-Qi, J. Tuck Samuel, and M. Corey Joseph. "Electrospinning Fundamentals: Optimizing Solution and Apparatus Parameters." *Journal of Visualized Experiements* 21, no. 47 (January 2011): 2494.

Li, D, and Y Xia. "Direct fabrication of composite and ceramic hollow nanofibers by electrospinning." *Nano Letters* 4, no. 5 (March 2004): 933-938.

Li, D, G Ouyang, J.T McCann, and Y Xia. "Collecting Electrospun Nanofibers with Patterned Electrodes." *Nano. Letters* (American Chemical Society) 5, no. 5 (April 2005): 913-916.

Ma, P.X, and Zhang, R. "Synthetic nanaoscale fibrous extracellular matrix." *Journal of Biomedical Materials Research* 46, no. 1 (July 1999): 60-72.

Matthews, J.A, G.E Wnek, D.G Simpson, and G.L Bowlin. "Electrospinning of collagen nanofibers." *Biomacromolecules* (American Chemical Society) 3, no. 2 (January 2002): 232-238.

Megelski, S, J.S Stephens, D.B Chase, and J.F Rabolt. "Micro- and nanostructured surface morphology on electrospun polymer fibers." *Macromolecules* (American Chemical Society) 35, no. 22 (September 2002): 8456-8466.

Mingjia, Zhi, Lee Shiwoo, Miller Nicholas, Menzler Norbert H., and Wu Niangiang. "An intermediate-temperature solid oxide fuel cell with electrospun nanofiber cathode." *Energy Environmental Science* 5 (March 2012): 7066-7071.

Mo, X. M., C. Y. Xu, M. Kotaki, and S Ramakrishna. "Electrospun P(LLA-CL) nanofiber: a biomimetic extracellular matrix for smooth muscle cell and endothelial cell proliferation." *Biomaterials* (Elsevier) 25, no. 10 (May 2004): 1883-1890.

Niklason, L.E. "Engineering of bone grafts." *Nature Biotechnology* 18, no. 9 (September 2000): 929-930.

Ondarcuhu, T, and C Joachim. "Drawing a single nanofibre over hundreds of microns." *Europhysics Letters* 42 (February 1998): 215-220.

Park, C, et al. "Polymer-single Wall Carbon Nanotube Composites for Potential Spacecraft Applications." *Materials Research Society Symposium Proceedings* 706 (2001): Z3.30.1-Z3.30.6.

Reneker, D H, and I Chun. "Nanometer diameters fibers of polymer, produced by electrospinning ." *Nanotechnology* 7 (1996): 216-223.

Ryan, O'Hayre, Barnett M David, and Prinz B Frits. "The Triple Phase Boundary - A Mathematical Model and Experimental Investigations for Fuel Cells." *Journal of The Electrochemical Society* 152, no. 2 (2005): A439-A444.

Seeram , Ramakrishna, Fujihara Kazutoshi , Teo Wee-Eong, Lim Teik-Cheng, and Ma Zuwei. *An Introduction to Electrospinning and Nanofibers.* World Scientific Publishing Co. Pte. Ltd., 2005.

Seungdoo, Park, Vohs M John, and Gorte J Raymond. "Direct oxidation of hydrocarbons in a solid-oxide fuel cell." *Letters to Nature* 404 (March 2000): 265-267.

Son, W.K, J.H Youk, T.S Lee, and W.H Park. "Electrospinning of ultrafine cellulose acetate fibers: studies of a new solvent system and deacetylation of ultrafine cellulose acetate fibers." *Journal of Polymer Science; Part B: Polymer Physics* 42, no. 1 (January 2004): 5-11.

Thompson, C J, G G Chase, A L Yarin, and D H Reneker. "Effects of parameters on nanofiber diameter determined from electrospinning model." *The International Journal for the Science and Technology of Polymers* (Elsevier) 48, no. 23 (November 2007): 6913-6922.

Virkar, A V, J Chen, C W Tanner, and J W Kim. "The role of electrode microstructure on activation and concentration polarizations in solid oxide fuel cells." *Solid State Ionics* (Elsevier) 131, no. 1-2 (June 2000): 189-198.

Von Hagen, R, A Lepcha, M Hoffmann, M Di Biase, and S Mathur. "Morphology controlled electrospinning of V205 nanofibers and their gas sensing behaviour." Edited by Sanjay Mathur and Suprakas Sinha Roy. *Nanostructured Materials and Nanotechnology: Ceramic Engineering & Science Proceedings* 32, no. 7 (2011): 3-9.

Wnek, G.E, M.E Carr, D.G Simpson, and G.L Bowling. "Electrospinning of nanofiber fibriogen structures." *Nano Letters* 3, no. 2 (December 2003): 213-216.

Won, Keun Son, Ho Youk Ji, Seung Lee Taek, and Ho Park Won. "The effects of solution properties and polyelectrolyte on electrospinning of ultrafine poly(ethylene oxide) fibers." *The International Journal for the Science and Technology of Polymers* 45, no. 9 (April 2004): 2959-2966.

Xia, Y., et al. "One-Dimensional Nanostructures: Synthesis, Characterization, and Applications." *Advanced Materials* 15, no. 5 (March 2003): 353-389.

Yang, Q, et al. "Influence of solvents on the formation of ultrathin uniform poly(vinyl pyrrolidone) nanofibers with electrospinning." *Journal of Polymer Science; Part B: Polymer Physics* 42, no. 20 (October 2004): 3721-3726.

Ying, Yang, Liu Jianan, Jia Zhidong, Wang Liming, and Guan Zhicheng. "Effect of solution rate on electrospinning." *Annual Report Conference on Electrical Insulation and Dielectric Pheonomena.* 2007. 615-618.

Yuan, X, Y Zhang, C Dong, and J Sheng. "Morphology of ultrafine polysulfone fibers prepared by electrospinning." *Polymer International* 53, no. 11 (November 2004): 1704-1710.

Zeleny, J. "The Electrical Discharge from Liquid Points, and A Hydrostatic Method of Measuring the Electric Intensity at their Surfaces." *Physical Review* 3, no. 2 (1914): 69.

Zeng, J, et al. "Biodegradable electrospun fibers for drug delivery." *Journal of Controlled Release* 92, no. 3 (October 2003): 227-231.

Zhao, YY, QB Yang, XF Lu, C Wang, and Y Wei. "Study on correlation of morphology of electrospun products of polyacrylamide with ultrahigh molecular weights." *Journal of Polymer Science Part B: Polymer Physics* 43, no. 16 (2005): 2190-2195.

Zhong, K Kim, D Fang, S Ran, B.S Hsiao, and B Chu. "Structure and process relationship of electrospun bioabsorbable nanofiber membranes." *The Internationa Journal for the Science and Technology of Polymers* 43, no. 16 (July 2002): 4403-4412.

Appendix A: Sintered ceria XRD data summary

Sample	Peak	$2\theta_{ref}$	I_{max}	$2\theta_{Peak}$	FWHM	a	Imax*a
C1	1	28.94	24.30	28.92210	0.34010	0.61009	14.82521
C1	2	33.47	11.70	33.46220	0.24371	0.52623	6.15683
C1	3	47.89	39.40	47.86340	0.22899	0.67070	26.42558
C1	4	56.76	46.60	56.70940	0.31014	0.63768	29.71603
C1	5	59.49	15.30	59.45620	0.18401	0.45160	6.90943
C1	6	69.81	19.90	69.75240	0.20719	0.49336	9.81778
C1	7	77.06	39.00	77.03670	0.47537	0.58097	22.65775
C1	8	79.43	31.60	79.40450	0.27229	0.50451	15.94245
C1	9	88.80	45.40	88.75030	0.25789	0.60814	27.60969
C1	10	95.73	42.70	95.69860	0.29446	0.56183	23.99023
C2	1	29.00	30.40	28.96190	0.29457	0.63386	19.26934
C2	2	33.52	14.20	33.49930	0.18105	0.58548	8.31382
C2	3	47.91	52.80	47.88950	0.25494	0.75792	40.01818
C2	4	56.79	64.90	56.73760	0.19355	0.77112	50.04569
C2	5	59.51	18.50	59.49310	0.14141	0.57609	10.65768
C2	6	69.86	26.00	69.80090	0.19420	0.59504	15.47107
C2	7	77.07	55.20	77.06920	0.19698	0.69619	38.42952
C2	8	79.45	39.20	79.43750	0.18579	0.68738	26.94514
C2	9	88.79	64.30	88.77400	0.20128	0.70868	45.56800
C2	10	95.72	61.00	95.73090	0.17032	0.76103	46.42253
C3	1	29.09	15.40	28.98540	1.65763	0.45770	7.04858
C3	2	33.62	8.10	33.54570	0.24584	0.43413	3.51647
C3	3	47.94	27.70	47.93550	0.16160	0.59699	16.53673
C3	4	56.81	31.70	56.77850	0.20299	0.59147	18.74963
C3	5	59.54	12.10	59.52870	0.18038	0.31891	3.85877
C3	6	69.84	19.70	69.84920	0.11504	0.35666	7.02610
C3	7	77.16	30.70	77.11030	0.17979	0.53244	16.34575
C3	8	79.46	27.40	79.47730	0.12969	0.53756	14.72914
C3	9	88.81	32.50	88.79740	0.20438	0.59253	19.25719
C3	10	95.80	37.60	95.75330	0.19313	0.49035	18.43727

Appendix B: Sintered Nickel XRD data summary

Sample	Peak	$2\theta_{ref}$	I_{max}	$2\theta_{Peak}$	FWHM	a	Imax*a
N1	1	37.51	108.70	37.46490	0.40602	0.59259	64.41399
N1	2	43.51	239.20	43.49830	0.24752	0.69740	166.81832
N1	3	63.10	280.00	63.07950	0.25658	0.64566	180.78480
N1	4	75.66	206.60	75.61060	0.20816	0.46750	96.58447
N1	5	79.64	173.00	79.59770	0.21588	0.41333	71.50626
N1	6	95.31	153.20	95.23610	0.20271	0.24675	37.80225
N2	1	37.53	124.00	37.49630	0.37060	0.61256	75.95769
N2	2	43.56	267.70	43.52840	0.31097	0.66625	178.35459
N2	3	63.16	280.00	63.10900	0.27195	0.66256	185.51596
N2	4	75.66	199.00	75.63520	0.23548	0.48793	97.09767
N2	5	79.65	178.20	79.62540	0.25080	0.40373	71.94469
N2	6	95.25	164.90	95.26170	0.15851	0.24221	39.94092
N3	1	37.58	147.10	37.56620	0.28907	0.63809	93.86304
N3	2	43.63	315.70	43.59590	0.24004	0.70185	221.57373
N3	3	63.18	340.10	63.16380	0.36442	0.68271	232.18899
N3	4	75.70	237.60	75.68580	0.20147	0.56428	134.07222
N3	5	79.70	207.70	79.66630	0.36957	0.44325	92.06240
N3	6	95.31	180.20	95.30720	0.27798	0.30870	55.62756

Appendix C: PDF Card

C.1. Cerium oxide PDF Card

PDF#00-034-0394: QM=Star(S); d=Diffractometer; I=Diffractometer — **PDF Card**

Cerianite-(Ce), syn (Cerium Oxide) (FLU)

CeO_2

Radiation=CuKa1 Lambda=1.5405981 Filter=Graph

Calibration=Internal(Ag) 2T=28.555-141.566 I/Ic(RIR)=

Ref: Natl. Bur. Stand. (U.S.) Monogr. 25, v20 p38 (1983)

CAS#:1306-38-3

Cubic - Powder Diffraction, Fm3m (225) Z=4

CELL: 5.41134 x 5.41134 x 5.41134 <90.0 x 90.0 x 90.0> P.S=cF12 (Ca F2)

Density(c)=7.215 Density(m)=6.50A Mwt=172.12 Vol=158.46 F(16)=129.8(.0077,16/0)

Ref: Ibid.

NOTE: This yttria stabilized phase was prepared at NBS, Gaithersburg, MD, USA, by Dragoo, Domingues (1982) from co-precipitation of the oxides. The powder was calcined at 620 C and then formed into a billet without binder, isostatically pressed, and then hot-pressed in an alumina die for 30 minutes at 1350 C with an applied stress of 28 MPa. The structure of fluorite was determined by Bragg (1914). Pattern taken at 26(1) C. To replace 4-593.

Color: Light gray, yellowish brown

Strong Lines: 3.12/X 1.91/5 1.63/4 2.71/3 1.10/1 1.24/1 0.91/1 1.04/1

16 Lines, Wavelength to Compute Theta = 1.54059Å(Cu), I%-Type = Peak Height

#	d(Å)	I(f)	h	k	l	2-Theta	Theta	1/(2d)	#	d(Å)	I(f)	h	k	l	2-Theta	Theta	1/(2d)
1	3.1234	100.0	1	1	1	28.555	14.277	0.1601	9	1.1048	14.0	4	2	2	88.412	44.206	0.4526
2	2.7056	30.0	2	0	0	33.082	16.541	0.1848	10	1.0415	11.0	5	1	1	95.396	47.698	0.4801
3	1.9134	52.0	2	2	0	47.479	23.739	0.2613	11	0.9566	4.0	4	4	0	107.264	53.632	0.5227
4	1.6318	42.0	3	1	1	56.335	28.167	0.3064	12	0.9147	13.0	5	3	1	114.729	57.365	0.5466
5	1.5622	8.0	2	2	2	59.086	29.543	0.3201	13	0.9019	6.0	6	0	0	117.317	58.658	0.5544
6	1.3531	8.0	4	0	0	69.401	34.701	0.3695	14	0.8556	9.0	6	2	0	128.392	64.196	0.5844
7	1.2415	14.0	3	3	1	76.699	38.350	0.4027	15	0.8252	6.0	5	3	3	137.970	68.985	0.6059
8	1.2101	8.0	4	2	0	79.069	39.535	0.4132	16	0.8158	5.0	6	2	2	141.566	70.783	0.6129

C.2. Nickel oxide PDF Card

PDF#00-047-1049: QM=Star(S); d=Diffractometer; I=Diffractometer | **PDF Card**

Bunsenite, syn (Nickel Oxide) (HAL)

NiO

Radiation=CuKa1 Lambda=1.540598 Filter=Graph

Calibration=Internal(Si) 2T=37.248-111.122 I/Ic(RIR)=6.15

Ref: Martin, K., McCarthy, G., North Dakota State Univ., Fargo, ND, USA.

ICDD Grant-in-Aid (1991) CAS#:1313-99-1

Cubic - Powder Diffraction, Fm3m (225) Z=4

CELL: 4.1771 x 4.1771 x 4.1771 <90.0 x 90.0 x 90.0> P.S=cF8 (Cl Na)

Density(c)=6.807 Density(m)=7.75A Mwt=74.70 Vol=72.88 F(8)=258.6(.0039,8/0)

Ref: Ibid.

NOTE: Sample obtained from J.T. Baker Chemical Corporation. Sample annealed for 72 hours at 1100 C. Average relative standard deviation in intensity of the 5 strongest reflections for 3 specimen mounts = 1.1%. Validated by calculated pattern. To replace 4-835.

Color: Green

Strong Lines: 2.09/X 2.41/6 1.48/4 1.26/1 1.21/1 0.93/1

8 Lines, Wavelength to Compute Theta = 1.54059Å(Cu), I%-Type = (Unknown)

#	d(Å)	I(f)	h	k	l	2-Theta	Theta	1/(2d)	#	d(Å)	I(f)	h	k	l	2-Theta	Theta	1/(2d)
1	2.4120	61.0	1	1	1	37.248	18.624	0.2073	5	1.2058	8.0	2	2	2	79.408	39.704	0.4147
2	2.0890	100.0	2	0	0	43.276	21.638	0.2393	6	1.0443	4.0	4	0	0	95.058	47.529	0.4788
3	1.4768	35.0	2	2	0	62.879	31.439	0.3386	7	0.9583	3.0	3	3	1	106.992	53.496	0.5218
4	1.2594	13.0	3	1	1	75.416	37.708	0.3970	8	0.9340	7.0	4	2	0	111.122	55.561	0.5353